Title: The differentiation commitment point closes a proliferative window that controls the total number of terminally differentiated cells

Authors: Michael L. Zhao[1], Atefeh Rabiee[1], Kyle M. Kovary[1], Zahra Bahrami-Nejad[1], Brooks Taylor[1], and Mary N. Teruel[1,*]

Affiliations:
[1]Dept. of Chemical and Systems Biology, Stanford University, Stanford, CA

***Corresponding Author:** mteruel@stanford.edu

SUMMARY

Terminal cell differentiation is essential for developing and maintaining tissues in all multi-cellular organisms. However, when and how the opposing processes of proliferation and cell differentiation interact to regulate permanent exit from the cell cycle is not well understood. Using adipogenesis as a model system, we here measure cell cycle progression and terminal cell differentiation live in single cells. We show that terminal cell differentiation occurs through a probabilistic competition that can last over several cell cycles with progenitor cells deciding between three cell-fates: proliferation, differentiation, and quiescence. We identify a terminal differentiation commitment point during a lengthening G1-phase that completely and rapidly suppresses future cell cycles, thereby closing a proliferative window that controls the total number of terminally differentiated cells. The combination of a terminal differentiation commitment point and regulated duration of a proliferative window may allow organisms to precisely control tissue development and regeneration.

HIGHLIGHTS

- Progenitor cells decide to differentiate using a probabilistic competition process that typically occurs after multiple cell cycles during an increasingly longer G1 period
- The G1 cyclin-CDK inhibitor p21 is induced by PPARG and extends G1 duration, as well as triggers permanent cell-cycle exit once PPARG reaches the threshold for differentiation.
- The underlying system architecture allows organisms to control tissue size by controlling the number of progenitor cell divisions that occur before terminal differentiation

Terminal cell differentiation is essential for developing, maintaining, and regenerating tissues in all multi-cellular organisms and is the mechanism by which adipocytes (fat cells), neurons, skeletal muscle cells, and many other cell types in humans and other multicellular organisms are generated (Ruijtenberg and van den Heuvel, 2016). Typically, during terminal differentiation, precursor cells that were once proliferative permanently withdraw from the cell cycle. Failure of terminally differentiated cells to exit from the cell cycle can lead to cancer and metabolic disorders (Ghaben and Scherer, 2019; Ruijtenberg and van den Heuvel, 2016). Despite the importance of properly-timed cell cycle exit during terminal differentiation, when and how this permanent cell cycle exit is achieved is poorly understood.

We are using adipogenesis as a model for terminal cell differentiation because it is an experimentally-accessible system in which the cell cycle and terminal differentition have been shown to be linked both in vitro and in vivo (Jeffery et al., 2015; Tang et al., 2003). A particularly striking example of this link is that manipulating the cell cycle by knocking out the CDK inhibitors p21 and p27 in mice caused a several-fold increase in adipogenesis and overall fat mass (Naaz et al., 2004). Our study addresses four fundamental open questions: First, is there a defined number of cell cycles that occur before terminal differentiation (Jones et al., 2007; Tang et al., 2003), or is there instead a proliferative window with a regulated duration, which allows different numbers of cell cycles to occur before terminal cell differentiation and thereby allows progenitor cells to control of the total number of produced differentiated cells? Second, are the processes of cell cycle exit and terminal cell differentiation independent events or not (Buttitta and Edgar, 2007; Hardwick et al., 2015; Soufi and Dalton, 2016)? Third, if the two processes are indeed connected, when precisely during a series of cell cycles do progenitor cells commit to a terminally differentiated fate after a differentiation stimulus is applied? Fourth, what signaling mechanisms can robustly mediate and maintain the non-proliferative state of differentiated cells?

The questions we are addressing arise from preceding studies that found molecular links between the cell cycle and terminal differentiation. For example, MyoD, a key regulator of muscle differentiation that can upregulate the cyclin dependent kinase inhibitor, p21, and inhibit cell-cycle

activity in a p53-independent manner (Guo et al., 1995; Halevy et al., 1995). Similar links between CDK inhibitors and differentiation were reported in other terminally differentiated cells, suggesting parallel pathways as well as tissue-specific redundancy in coordinating cell cycle exit and terminal differentiation (Buttitta et al., 2007; Parker et al., 2006; Ruijtenberg et al., 2015; Zalc et al., 2014). There is also evidence that diffentiation is associated with a lenghteneing of G1 phase. For example, a recent study in human embryonic stem cells showed that a gain of differentiation markers coincide with G1 phase lengthening, and distinct G1 phase profiles are associated with different markers of early hESC differentiation (Calder et al., 2012). Another study showed G1 lengthening in pancreatic progenitor cells, where it helps stabilize NEUROG3 during cell differentiation (Krentz et al., 2017), and G1 lengthening was also shown to be help switch neural progenitors to neurogenesis (Lange et al., 2009).

However, even though molecular links have been found between terminal differentiation and cell cycle lengthening/exit, there is conflicting evidence on whether and how strongly the two processes are connected. For example, studies in adipocytes and neurons sugegsted that G1-lengthening, cell cycle exit, and terminal differentiation happen sequentially (Lange et al., 2009; Tang et al., 2003) whereas other studies support model that cell cycle exit and differentiation occur as parallel, independently-regulated processes (Lacomme et al., 2012; Qiu et al., 2001). Still other studies suggest that the two processes are co-coordinated by dual actions of core components of the cell cycle and differentiation machinery (Hardwick et al., 2015).

One challenge in understanding the relationship between cell cycle exit and differentiation is that there is great variability whether and when individual progenitor cells in the same population proliferate or differentiate during the several-day long differentiation process. To overcome this challenge, methods are needed that can capture whether and when an individual cell decides to irreversibly differentiate and permanently exit the cell cycle, while at the same time tracking the cell cycle and differentiation progression during the multi-day long differentiation timecourse. Live-cell imaging approaches have been applied to stem cells that undergo a slowing or transient exit from the

cell cycle during the differentiation process (Matson et al., 2017; Pauklin and Vallier, 2013). However, live-cell imaging studies to understand the timing of cell cycle exit during terminal cell differentiation have to our knowledge not yet been made, and the underlying regulatory mechanisms could be different when a permanent rather than temporary cell cycle exit is required. To establish whether there is a direct link between the cell cycle and terminal cell differentiation, it is necesssary to mark with a live-cell marker not only G1 phase but also the precise time when a cell irreversibly commits to terminally differentiate and such a marker did to our knowledge not yet exist.

Many terminal cell differentiation systems including adipogenesis and myogenesis are regulated by a cascade of transcription factors (Blais et al., 2005; Farmer, 2006). In order to establish a temporal marker for differentiation commitment, it is essential to determine which of the factors in the transcriptional cascade controlling differentiation process exhibits bimodal and irreversible behavior and can thus be used to distinguish whether a cell still has the option to remain undifferentiated or has committed to terminally differentiate. For example, in adipogenesis, even though the early transcription factor CEBPB is required, it is not a suitable marker of differentiation commitment. CEBPB levels increase in all cells that are subjected to the DMI adipogenic stimulus, but the levels are not predictive of whether or not a cell will continue on to differentiate once the stimulus is removed (Bahrami-Nejad et al., 2018). Previous work using single-cell imaging showed that the transcription factor PPARG exhibits bimodal, irreversible behavior and suggested that the level of PPARG can distinguish undifferentiated from differentiated cells (Ahrends et al., 2014; Bahrami-Nejad et al., 2018; Park et al., 2012) (Figures 1A-C).

Here we investigate how mitogen and differentiation stimuli control the terminal cell differentiation process. We start by showing that a threshold level of endogenously tagged PPARG protein can be used in live cells to mark the precise time when cells irreversibly commit to differentiate, and we establish a method to simultaneously track the cell-cycle and terminal cell differentiation in the same cell. We then show that proliferation and terminal cell differentiation are directly linked, with cells being prevented during the S/G2/M phases of the cell cycle from reaching the PPARG threshold for

terminal differentiation. Cells only reach the PPARG threshold to terminally differentiate during a progressively longer G1 phase by increasing the expression and life-time of the CDK inhibitor p21, which forces permanent exit from the cell cycle. Importantly, we show that cells compete during the G1 phase between (1) reaching the terminal differentiation commitment point and closing the window of proliferation or (2) reaching the start of the next cell cycle and extending the window of proliferation to allow for more cell cycles to occur. Together, our study shows that in order to optimally control how many terminally differentiated cells are produced, the cell cycle and differentiation processes have to both be manipulated in parallel in order to regulate not only how many cell cycles occur before terminal differentiation but also when the differentiation commitment point is reached and the proliferative window closes.

RESULTS

Live-cell analysis of the precise time when preadipocytes commit to the terminally differentiated state

A major bottleneck in understanding the relationship between the cell cycle and terminal cell differentiation is the lack of a quantitative live-cell readout that marks the precise time point when a cell commits to the terminally differentiated state (Buttitta and Edgar, 2007). We start by establishing such a live-cell readout that marks the commitment point for terminal cell differentiation. We are using adipogenesis as a cell model since many regulators of adipocyte differentiation are known, since the validity of in vitro cell models for adipogenesis studies has been corroborated by in vivo studies (Ghaben and Scherer, 2019), and since previous in vitro and in vivo studies provided evidence that the cell cycle has a role in regulating adipogenesis (Jeffery et al., 2015; Tang et al., 2003). Adipogenesis is centered on a master transcriptional regulator, PPARG, whose expression is driven by both external input signals and internal positive feedback loops (Ahrends et al., 2014; Rosen and Spiegelman, 2014) (Figure 1A, top). In previous work, we used CRISPR-mediated genome editing to fluorescently tag endogenous PPARG as a live-cell readout of differentiation progression (Bahrami-

Nejad et al., 2018). To enable automated nuclear tracking of moving cells, we also stably transfected the cells with fluorescently labeled histone H2B (Figure 1A, bottom). We now go on to determine whether fluorescently-tagged endogenous PPARG can be used to measure a threshold level of PPARG expression that marks in live cells the precise time point when an individual cell irreversibly commits to the terminally differentiated state.

To induce differentiation, we applied a commonly used adipogenic hormone cocktail (DMI, see Methods) that mimics glucocorticoids and GPCR-signals that raise cAMP. DMI is applied for 48 hours to preadipocytes and then replaced for another 48 hours with refreshed growth medium containing insulin to test for terminal differentiation at 96 hours. The removal of DMI is critical since it allows for a determination whether a cell can continue on to reach and maintain a distinct terminally differentiated state two days later (Figure 1B). Indeed, this protocol produces two distinct outcomes for cells, one group of cells that keeps increasing PPARG levels after removal of the differentiation stimulus (Figure 1B, blue traces), whereas PPARG levels of cells in the other group fall back to the undifferentiated precursor state (Figure 1B, orange traces). When analyzed at 96 hours using a histogram that groups the number of cells at increasing levels of PPARG expression, the single-cell distribution of PPARG levels is bimodal with a high peak in the histogram representing the differentiated cells and a low peak the undifferentiated cells (Figure 1B, right-side histogram).

To determine whether a defined PPARG threshold exists at 48 hours that predetermines the subsequent two cell fates at 96 hours, we compared in live cells the PPARG levels at 48 hours - before DMI was removed - to the PPARG level in the same cell at 96-hour. Indeed, the level of PPARG at 48 hours can predict with a less than 5% false positive rate whether a cell keeps increasing PPARG and terminally differentiate or falls back to the level of progenitor cells (Figures 1B-C, black dashed line). Furthermore, PPARG levels are directly correlated with a set of commonly used markers of differentiated adipocytes at the single-cell level (Figure 1D), further arguing that the PPARG threshold marks an irreversible commitment point for terminal differentiation (see Methods section for details of how the threshold is calibrated in each experiment).

In additional control experiments, we determined how predictable PPARG levels are at 24, 48 or 72 hours of stimulation of cell fate at 96 hours. As shown in Figure 1E, cells that increase PPARG earlier have a higher probability to ultimately differentiate, and cells will terminally differentiate close to 100% once PPARG levels increase 50% above the threshold, independent of whether cells have reached the PPARG threshold at 24, 48 or 72 hours (see also Figure S1). Furthermore, the probability to differentiate did not exhibit a significant dependence on PPARG levels at the start of the experiment (Figure 1E), showing that terminal differentiation is variable between cells due to variable responsiveness to DMI rather than being predetermined by basal PPARG levels.

Finally, terminal cell differentiation of adipocytes is mediated by a positive feedback-driven bistable switch mechanism between PPARG and several co-regulators that together amplify PPARG expression. To determine whether the PPARG threshold marks the time when the bistable switch is triggered, we computationally aligned single-cell traces to the time when each cell crosses the PPARG threshold. Consistent with the hypothesis that the PPARG threshold marks the time when the bistable PPARG switch mechanism is triggered, the aligned cells show a sharp sigmoidal increase from a slow rate of PPARG increase before the PPARG threshold to a fast rate after that time point (Figure 1F; Figure S2A). The same alignment to the PPARG threshold (blue traces, Fig 1G) also allowed us to determine how correlated the increasing PPARG level is with the final measurement of a set of commonly used markers of differentiated fat cells at 96 hours. Indeed, only when a cell crosses the PPARG threshold, become PPARG levels significantly correlated with markers of mature adipocytes two days later (red traces), supporting the conclusion that crossing the PPARG threshold marks a short time window of PPARG self-amplification that causes an irreversible commitment to the future terminally differentiated adipocyte state.

Taken together, these different experiments validate that a PPARG threshold level can be used to mark a precise time when precursor cells commit to terminally differentiate even before the markers of mature fat cells can be measured. When adipogenic stimuli are removed, cells that passed the PPARG threshold go on to terminally differentiate two days later, while cells below the threshold

return to the undifferentiated progenitor state. Thus, fluorescently-tagged endogenous PPARG can be used to directly address the question what the connection is between the decisions to terminally differentiate and to permanently exit the cell cycle.

Simultaneous single-cell analysis shows that further entry into the cell cycle is blocked once a cell reaches in G1 the differentiation commitment point

In order to monitor cell cycle progression and the commitment to terminally differentiate simultaneously in the same cells, we made a dual-reporter cell line by transfecting a FUCCI cell-cycle reporter (Sakaue-Sawano et al., 2008) into OP9 preadipocyte cells expressing endogenous citrine-PPARG (Figure 2A). The FUCCI cell-cycle reporter is composed of a red fluorescent protein mCherry fused to a fragment of the geminin protein that is degraded by both anaphase promoting complex/cyclosomes (APC/C). Specifically, the reporter signal rapidly drops when cells activate the first E3 ubiquitin ligase APC/C^{CDC20} in mitosis before cells start G1 phase, and the signal only starts to increase close to the end of G1 phase when the second APC/C^{CDH1}, which is active during G1, is rapidly inactivated (Cappell et al., 2016). To validate that the geminin degron sensor is suitable to monitor G1 length in the OP9 preadipocyte cell system, we compared its dynamics to that of a reporter of CRL4-Cdt2-mediated degradation that provides a more precise measure of the G1/S transition (Grant et al., 2018; Sakaue-Sawano et al., 2017) and confirmed that the increase in expression of the geminin degron sensor and degradation of the CRL4-Cdt2 sensor are closely correlated in these cells (Figure S2). Thus, the dual-reporter system can be used to simultaneously monitor the commitment to the terminally differentiated state as well as the start of G1 and G1 length. Furthermore, in the following experiments, we purposely used sub-confluent cell plating conditions in order to maximize the number of cell divisions, to reduce the effect of cell density on cell cycle arrest, and to improve the fidelity of the automated tracking algorithm (Figure S3A-B).

To determine when terminal cell differentiation occurs relative to the last cell cycle, we tracked PPARG expression levels and geminin reporter time courses over four days of differentiation.

Trajectories of cells in the population that terminally differentiate were marked in blue, and cells that stayed in the progenitor state in orange (Figure 2B). The trajectories show that cells that terminally differentiate have fewer cell cycles and exit the last mitosis earlier (Figures 2B-C) compared to cells that are not undergoing terminal differentiation. Such an inverse relationship between proliferation and terminal cell differentiation can be represented in a cumulative plot comparing the percent of cells still in S/G2/M versus the percent of cells that have crossed the PPARG threshold for terminal differentiation, as a function of time after DMI stimulation (Figure 2D). Control experiments showed no significant differences in PPARG levels between cells that underwent two versus three cell cycles which argued against the possibility that the lower differentiation observed in cycling cells was due to PPARG simply being diluted more in cells that cycle more often (Figure S3C-D).

When visually inspecting hundreds of single-cell traces, we found great variability in the kinetics of PPARG increases and cell-cycle responses (Figure 2E). However, no new cell-cycle entry was observed if the PPARG level in a cell increased above the threshold for terminal differentiation (marked with a yellow dot, Figure 2E), arguing that permanent cell-cycle exit is forced on cells when they reach the commitment point to terminally differentiate. We observed that PPARG levels already increase in many cells during S/G2/M phase of the cell cycle, but a large majority of differentiating cells only reach the PPARG threshold for terminal differentiation in G1 phase. Control experiments using a CDK2 activity reporter (Spencer et al., 2013) instead of the geminin sensor confirmed that commitment to terminally differentiate happens during G1 phase, as shown by the fact that PPARG levels are only high when CDK2 activity levels are low (Figure S3E-F). Perhaps the clearest relationship between terminal differentiation and the last mitosis can be seen in a histogram analysis of when relative to the last mitosis each cell commits to a terminally differentiated state. While cells pass the commitment point for terminal differentiation at different times, almost all do so only after mitosis and the average time to commitment is approximately 14 hours from the last mitosis (Figure 2E). Thus, cells commit to the terminally differentiated state almost exclusively in G1.

An interesting result from this analysis was that preadipocytes undergo a variable number of

cell divisions before they differentiate (Figures 2C and 2E), arguing that terminal differentiation of adipocytes does not occur after a fixed number of cell divisions before differentiation as has been previously suggested (Tang et al., 2003). Since the previous study relied on averaged, population-based measurements, the variable number of mitoses in different cells could likely not be resolved without live single-cell analysis. Not only the number of cell cycles can vary, it is also apparent from the time courses in Figure 2E that there is great variability in the time after stimulation when cells start to increase PPARG levels, and also in the time cells spend in G1 before cells reach the PPARG threshold for terminal differentiation. Finally, the hypothesis that differentiation stimuli induce the PPARG expression program more effectively during G1 is also supported by the finding that cells differentiate more effectively if the differentiation stimulus was added to cells in G1 compared to cells in S/G2/M (Figure S4).

We conclude that terminal adipocyte differentiation occurs after a variable rather than fixed number of cell cycles, that most preadipocytes reach the commitment point for terminal differentiation after spending variable times in G1, that cells partially suppress the increase in PPARG during S/G2/M, and that cells permanently exit the cell cycle at the same time when they pass the commitment point for terminal cell differentiation.

PPARG regulates terminal cell-cycle exit by inducing p21 and FKBPL

A question raised by the time-course data is if and how PPARG may lengthen G1 and cause permanent cell cycle exit since only DMI-stimulated cells that continuously proliferate consistently have low levels of PPARG (Figures 2B and 2E). To test for a direct role of PPARG in suppressing proliferation, we used siRNA targeting PPARG to determine whether this relationship is causative. Indeed, even the relatively small increase in PPARG before cells reach the threshold for differentiation has an inhibitory effect on the cell cycle since siRNA knockdown of PPARG increases the percent of proliferating cells from the start throughout the time course of differentiation (Figure 3A). Based on our observation that differentiation commitment occurs only out of a state with low CDK2 activity (Figure

S4A-B), we thus hypothesized that PPARG may increase the expression of one of the CDK inhibitors, and that CDK inhibitors may then slow or inhibit entry into the next cell cycle.

We sought to identify putative inhibitors of proliferation by performing RNA-seq analysis on cells transfected with siRNA targeting PPARG, or control siRNAs, and collected the transcripts at different timepoints during a 144-hour DMI differentiation protocol. We examined mRNA expression profiles of canonical CDK inhibitors and identified two that were strongly regulated by PPARG expression, p18 and p21 (Figure 3B). A PPARG-mediated increase in p21 has also been reported in other cell types (Han et al., 2004). To validate that p18 and p21 could mediate cell-cycle arrest during adipogenesis, we carried out siRNA knockdown experiments and found that p21, but not p18, knockdown led to an increase in proliferation (Figure 3C). We tested whether the effect from PPARG on p21 is direct by adding rosiglitazone, a small molecule that directly activates PPARG, which led to a robust increase in p21 expression (Figure 3D). Experiments in which p21 was knocked down with siRNA showed that p21 is required for PPARG to mediate both terminal cell differentiation as well as suppression of proliferation (Figure 3E). Furthermore, ChiP-Seq experiments support that PPARG directly increases p21 expression since there was significant binding of PPARG to the promoter of p21 during adipogenesis induced by DMI stimulation (Figure 3F).

In the same RNA-seq data, we also found that PPARG increases the expression of FKBPL (WiSP39), a protein that was shown to stabilize p21 and increase the ability of p21 to arrest cells in response to ionizing radiation (Jascur et al., 2005)(Figure 3G). To test if p21 could be stabilized by FKBPL during the early stages of adipogenesis, we carried out cycloheximide protein degradation experiments to measure the half-life of p21 in cells transfected with siRNA targeting FKBPL. Our results showed that knockdown of FKBPL decreased p21 half-life but did not affect the half-life of PPARG, supporting that FKBPL does regulate p21 stability during terminal cell differentiation (Figure 3G). Taken together, our results demonstrate that PPARG slows and stops proliferating cells in G1 in part by increasing p21 levels by (i) directly increasing p21 transcription and (ii) FKBPL-mediated slowing of p21 degradation.

The commitment to terminally differentiate coincides with a CDK inhibitor-mediated terminal exit from the cell cycle

We next focused on the question how preadipocyte cells trigger permanent exit from the cell cycle once they pass the PPARG threshold for terminal differentiation. To determine the relationship between PPARG levels and terminal cell cycle exit, we took advantage of the variable increase in PPARG following DMI stimulation and grouped cells into 10 bins according to their expression level of PPARG at 48 hours (Figure 4A). At this 48-hour timepoint, the media was changed from DMI to media with insulin and growth factors and no differentiation stimuli. The corresponding mean PPARG (left) and geminin-degron (right) signals were plotted for each bin. We found that the group of cells that passed the PPARG threshold, but not the cells that stayed below the threshold, showed no significant geminin signal in response to fresh growth media, demonstrating that cells lose the ability to re-enter the cell-cycle entry after they cross the threshold for terminal differentiation. We confirmed that this is indeed the result of reduced cell-cycle activity by calculating the fraction of cells that underwent mitosis in response to fresh growth media (Figure 4B, red). Thus, cells that pass the PPARG threshold lose the proliferation response to freshly-added growth factors, arguing that crossing the PPARG threshold marks the time when cells permanently enter a post-mitotic state.

We next investigated how p21 levels change relative to PPARG levels in individual cells. After completion of a live cell time course, we fixed and stained cells for p21 expression. We again binned cells according to PPARG levels and plotted the mean nuclear p21 fluorescence for each bin (Figure 4B, black). We found that p21 levels gradually increase along with PPARG until the PPARG threshold after which p21 plateaus and stays high, suggesting that p21 is not only lengthening G1 but also maintaining the postmitotic state.

To directly test for such a maintenance role of p21, we added siRNA to knockdown p21 only late in adipogenesis at the 48-hour timepoint when the adipogenic stimulus was replaced with growth factor containing media. As a control, we also started at the same time to knock down PPARG and

CEBPA, a required co-activator of PPARG expression that is needed for cells to reach the threshold for differentiation (Bahrami-Nejad et al., 2018; Wu et al., 1999). Acute knockdowns of all three regulators after the commitment point to terminally differentiate showed that only p21 knockdown resulted in a significant increase in cell-cycle activity (Figure 4C). To quantitatively analyze this result, we grouped cells by their PPARG levels and plotted the average time course for each group during the removal of DMI and addition of growth factors. As expected, control experiments show that if PPARG levels are above the threshold, geminin signals remain suppressed, consistent with a lack of proliferation. However, acute knockdown of p21 expression led to a loss of the ability of PPARG levels to suppress geminin signals and maintain the postmitotic state even though PPARG levels stayed above the threshold (Figure 4D). This loss of maintenance of the postmitotic state can also be seen in an analysis showing the percent of cells in the cell cycle in Figure 4E. Thus, a maintained high level of p21 is required for cells to maintain the post-mitotic state after cells passed the commitment point for terminal cell differentiation.

Notably, when we examined images of cells from Figure 4E that had p21 depleted after crossing the commitment point, we found that PPARG high cells were enriched for multinucleation events (Figure 4F). This suggests that a critical role of p21 is to permanently prevent cell division after terminal differentiation to prevent mitotic defects.

Finally, it was recently shown that the ratio of nuclear expression of cyclin D1 versus p21 can control Rb hyperphosphorylation and re-entry into the cell cycle (Yang et al., 2017). We determined whether the role of the PPARG-induced increase in p21 expression is to shift this p21-cyclinD1 ratio towards high p21 to keep Rb dephosphorylated and ensure that cells remain unresponsive to serum stimulation. As shown in a plot of p21 versus cyclinD1 levels in a large number of single cells (Figure 4G), the ratio of p21 to cyclinD1 becomes strongly skewed towards p21 when PPARG levels go above the threshold during adipogenesis, providing an explanation of how differentiated cells can maintain a robust arrested state. Taken together, our data shows that the commitment to terminally differentiate also marks entry into a permanent post-mitotic state, and that p21 is needed to maintain the health of

terminally differentiated cells by preventing cells in the postmitotic state from proliferating after commitment.

An ongoing race during G1 between differentiation and closing the window of proliferation or keeping the window open by entering the next cell cycle

Previous live-cell analysis of the cell cycle in the differentiation of stem cells, which do not terminally differentiate, has shown that cells temporally lengthen G1 as part of the differentiation process (Matson et al., 2017). The relationship between G1 lengthening and differentiation is less well understood for terminal cell differentiation, and we first determined whether a gradual lengthening of G1 already occurs in the cell cycles that precedes the G1 phase from which cells terminally differentiate. Preadipocytes can undergo rapid cell cycles with a G1 phase that is on average only about 4 hours (Figure 5A). However, more than 14 hours on average is needed after the last mitosis in order for a cell to reach the PPARG threshold for terminal differentiation (Figures 2F and 5A), arguing that G1 must be lengthened before progenitor cells can commit to terminally differentiate.

We had observed that the duration of G1 versus S/G2/M phases was longer after DMI-induced differentiation for cells in Figure 2B (Figure S6A). To test whether the adipogenic stimuli were triggering a gradual lengthening of G1 over time, or only a single G1 extension when they terminally differentiate, we selected cells that underwent three mitoses following DMI stimulation and before terminal differentiation, and compared the G1 duration for the first and second observed G1 phase ($G1_1$ and $G1_2$, see scheme in Figure 5B, left). Consistent with a DMI-induced gradual lengthening of G1, the second G1 length is typically significantly longer (Figure 5B, right; Figure S6B). When G1 length is plotted as a function of the time after DMI stimulation, the length of G1 initially can be seen to increase gradually from 12 to about 18 hours and more strongly from 18 to about 30 hours (Figure S6C). Thus, adipogenic stimuli progressively lengthen their G1 period before cells reach the last mitosis and then terminally differentiate out of the last G1 phase.

This DMI-induced G1 lengthening raises the question whether the reason why cells do not

differentiate more quickly after DMI stimulation is simply the result of cells having a short G1 period for the first few cell cycles so that PPARG can be mostly suppressed during S/G2/M. To test whether there is a delay before cells activate PPARG that is independent from the lengthening of G1, we made use of the high variability in cell cycle responses in the cell population. By computationally aligning the time-courses by the time a cell completes its last mitosis, we were able to measure more precisely PPARG increases before and after the last mitosis (Figure 5C). If a cell had a last mitosis in the first 12 hours after DMI addition, PPARG did not noticeably increase both before or within 12 hours after mitosis. If a cell had its last mitosis 12-24 hours after DMI addition, PPARG showed only a small increase but only after mitosis. Markedly, this increase of PPARG after mitosis becomes stronger when a cell had its last mitosis 24-36 hours after DMI addition. Thus, there is a delay mechanism that is independent of the cell cycle that restricts the increase in PPARG not only to the G1 phase but also to a time window starting only at approximately 24-36 hours after DMI stimulation.

To more directly evaluate the delay before PPARG can increase in G1, we made the same alignments but with smaller time windows and by measuring the time each cell takes after mitosis to reach the PPARG threshold. We used the timecourse data shown in Figure 2B and binned cells into groups based on when a cell completed its last mitosis in increments of 4 hours (see scheme in Figure 5D). The data shows that the later a cell exited the last mitosis, and thus the longer the proliferating cell was exposed to the adipogenic stimuli, the less time a cell needed to spend in G1 before reaching the PPARG threshold (Figure 5E, left). Furthermore, cells that spend less time in G1 are less likely to terminally differentiate (Figure 5E, right), consistent with a critical repressive contribution from the ongoing S/G2/M part of the cell cycle to terminal differentiation.

Taken together, our data can be summarized in the following model for terminal cell differentiation of adipocytes (Figure 5F): DMI stimuli cause preadipocytes to first enter a proliferative time window with short G1 periods. The differentiation program only slowly engages by gradually accelerating the rate of PPARG increase to the threshold as well as by gradually extending G1 length. This is setting up a race after the end of each mitoses as to whether a cell first reaches the commitment

to terminally differentiate, which then closes the proliferative window and suppresses future cell cycles, or cells first commit to the next cell cycle at the onset of S phase, which extends the proliferative window at least until the next mitosis. Thus, at the end of an extended G1 phase, cells will either (1) terminally differentiate, (2) remain proliferative and undifferentiated or (3) cells can also end-up in a quiescence progenitor state, which will be discussed further below.

Regulation of duration of the proliferative window differentially controls the percent versus total number of terminally differentiated cells

Given our observation that cells can have variable numbers of cell cycles before terminal cell differentiation, or keep proliferating after removal of the adipogenic stimulus, made us directly test whether the percent of cells that will terminally differentiate can be controlled by lowering growth factor stimuli or by directly manipulating the levels of the G1 phase regulators cyclin Ds and p21. To directly test the model that receptor-tyrosine kinase signaling pathways may regulate proliferation and terminal differentiation in different ways, we first focused on the EGF receptor and the Ras/MEK/Erk signaling pathway. Indeed, when we either stimulated cells with DMI along with EGF or no EGF (cells were in 2% FBS to maintain cell health) (Figure 6A), we observed more cells proliferated for longer upon stimulation with EGF and, less predictable, EGF also reduced the percentage of cells that terminally differentiated. Furthermore, addition of MEK inhibitor along with DMI under full serum conditions not only shortened the window of proliferation but also caused a parallel increase in the percentage of terminally differentiated cells (Figure 6B).

Nevertheless, the EGFR and the MEK/ERK signaling pathways have many targets and may separately regulate differentiation and proliferation processes. In its role to regulate proliferation, the EGFR-MEK-ERK pathway is known to increase the expression of cyclin D1, and also reduce expression of p21 and p27, which both promote Rb hyperphosphorylation and cell proliferation. One of the most striking findings from gene knockout studies was that fat tissues of female mice with deleted CDK inhibitors p21 and p27 show a 5-fold disproportionate enlargement of fat mass. This

earlier finding was unexpected, since one may have expected that the increase in proliferation resulting from the loss of CDK inhibitors should yield less terminally differentiated cells and not more.

To directly test whether knockdown of p21 in preadipocytes could recapitulate this in vivo result, we knocked down p21 and confirmed that cells spend overall less time in G1 phase, consistent with p21 functioning as an inhibitor of proliferation that lengthens G1 (Figure 6C, left). This decrease in G1 duration was associated with the same increase in the percent of proliferating cells similar to the effect of EGF stimulation, and also resulted in a decrease in the percent of differentiated cells, which can again be explained by short G1 periods giving less opportunity for PPARG levels to increase during each G1 (Figure 6C, middle). However, when we analyzed the total number of differentiated adipocytes, the number increased significantly in the p21 knockdown condition (Figure 6C, right). The increase in the total number of terminally differentiated cells can be explained by an increase in the number of cell divisions during the proliferative window before cells close the window when they reach the PPARG threshold. Conversely, overexpressing p21 using a DHFR induction system yielded the opposite effect: the percent of proliferating cells decreased and there was a corresponding small increase in average PPARG expression and lower total number of differentiated cells (Figure 6D). Thus, the puzzling finding of high fat mass and adipocyte number in mice lacking p21/p27 type CDK inhibitors can be explained in the in vitro analysis by progenitor cells undergoing more cell cycles in the absence of CDK inhibitors before they terminally differentiate and thereby increase the total number of produced adipocytes.

Since a second role of the EGF and Ras/MEK/ERK pathway is also to increase cyclin D1 expression, we also tested the effect of reducing cyclin D1 expression on the total number of differentiated cells produced. Consistent with our model of an increase in G1 duration allowing more cells to build up PPARG levels and differentiate, we found that cyclin D1 knockdown led to an increase in G1 duration, lowered cell cycle activity, and increase in the percent differentiated cells (Figure 6C). The kinetics when cells differentiated was different from the case of p21 overexpression experiments in that many cells differentiated earlier but fewer differentiated later, but the analysis showed a similar

phenotype at 96 hours with fewer total differentiated cells produced. The observed kinetic differences may in part result from additional roles that cyclin Ds may have in regulating differentiation that do not work through regulation of CDK4/6 (Fu et al., 2005). Together, these findings are consistent with the interpretation that cyclin D1 and p21 act in opposite direction to control the length of G1 as well as the duration of the proliferative window.

Together, these experiments show that the CDK inhibitor p21 and cyclin D play critical opposing roles in terminal differentiation by regulating not only the percentage of progenitor cells that terminally differentiate as but also the total number of differentiated cells. It is thus plausible that altering signaling pathways that selectively change expression of different cyclin Ds or CDK inhibitors may be therapeutically useful to synergistically control terminal cell differentiation by independently regulating the percentage and total number of terminally differentiated cells.

Different optimal ranges of mitogenic and differentiation stimuli control the percent and total number of terminally differentiated cells

Mammals have a large pool of preadipocytes near the vasculature of most tissues, and fat tissue is replaced at a low rate which makes adipogenesis to be a relatively slow process with only a percentage of progenitor cells proliferating and differentiating at a given time. How cells are regulated by mitogen and differentiation stimuli is therefore an interesting question since there are unique regulatory features of terminal cell differentiation that do not apply to differentiation processes such as stem cell differentiation and neuroendocrine cell differentiation which do not initially end in a postmitotic state (Krentz et al., 2017; Liu et al., 2019; Miyatsuka et al., 2011). As diagrammed in Figure 7A for terminal cell differentiation, the differentiation stimulus starts a proliferative window whose duration can be regulated by cyclin D, p21 and other factors and which only closes when cells reach the commitment point for terminal differentiation, thus allowing for a regulation of the number of cell divisions before terminal cell differentiation.

Therefore, organisms may regulate the total number of adipocytes they produce in two ways: First, organisms can regulate the percent of progenitor cells that terminally differentiate since individual cells have variable signaling sensitivity so that increasing the strength of adipogenic stimuli causes an increase of the percent of progenitor cells in a population that differentiate (Ahrends et al., 2014; Park et al., 2012). Second, the duration of the proliferative window of individual progenitor cells can be regulated and, if the window is longer and more cell cycles can occur before terminal differentiation commitment, then the total number of daughter cells increases, and also more differentiated cells can be generated from the same number of activated progenitor cells. For example, an example shown in the scheme in Figure 7B shows has 2 cell divisions, a final outcome of 50% differentiated cells, and 2 total fat cells produced. In the other example with 3 cell divisions, the final cell population is also 50% differentiated cells but a total of 6 adipocytes are produced.

In this way, if a tissue needs more differentiated cells, why not just keep increasing the proliferative window before differentiation? An additional outcome is that progenitor cells can also return to the quiescent state before they differentiate due to inhibitory signals from sources such as the differentiation stimulus itself, increased cell contact and stress, and once cells are quiescent for longer time periods, they are expected to become less capable to differentiate compared to cells that recently proliferated since proliferation has been shown to mediate epigenetic reprogramming needed for cell differentiation. For the DMI stimulation protocol we mostly used, there are approximately 35% of progenitor cells becoming quiescent without undergoing terminal differentiation (Figure 7C). Thus, one would expect that the relative strength of proliferation and differentiation signals that maximizes the percent of cells that differentiate should be different from the relative strength that maximizes the total number of differentiated cells produced.

To test this hypothesis, we performed experiments in which we systematically applied different relative strengths of adipogenic and mitogenic stimuli for 48 hours and then removed the stimulus such that we could determine at 96 hours (i) the total number of cells, (ii) the percentage of terminally differentiated cells, and (iii) the total number of terminally differentiated cells. When focusing on the

total number of cells at the end of the experiment, higher mitogen stimuli invariably increased the total number of cells produced independently of the strength of the adipogenic stimulus. In contrast, since adipogenic stimuli suppress proliferation, the total number of cells decreased for increasing adipogenic stimuli. When focusing on the percent of cells that end up terminally differentiated, higher adipogenic stimuli invariably increased the percent of cells that end up terminally differentiated independent of the strength of the mitogen stimulus. Since proliferating cells inhibit differentiation, the percent of differentiated cells is nevertheless also reduced with increasing mitogen stimuli which is particularly clear for the higher DMI stimuli. As a consequence of the dual regulation, combined mitogen and adipogenic stimuli result in an overall triangular effect on the total number of differentiated cells, with higher mitogen and higher adipogenic stimuli synergistically increasing the total differentiated cells produced from the same number of progenitor cells. At the highest levels of mitogen and adipogenic stimuli, maximal adipogenic stimuli start to reduce the total number of differentiated cells, suggesting that there can be optimal ranges of mitogen and adipogenic stimuli that maximize the number of terminally differentiated cells.

We conclude that terminal cell differentiation is based on a race between mitogens and adipogenic stimuli to drive a competition in G1 between cells to either reach the commitment point for terminal differentiation, which can close the proliferative window early, or to start the next cell cycle, and extend the window of proliferation by allowing more cell divisions. Particularly for lower differentiation and mitogen stimuli, cells also eventually exit the differentiation program to a quiescent, undifferentiated progenitor state.

DISCUSSION

Using adipogenesis as a model system for terminal cell differentiation, we have carried out live single-cell analysis to determine the molecular mechanisms and timing between cell-cycle exit and terminal cell differentiation. Our study highlights advantages of studying terminal differentiation in adipocytes as we were able to develop a live molecular marker to precisely determine when cells

make the transition to the terminally differentiated state. We showed that the decision to terminally differentiate in cells is made out of a lengthening G1 phase after cells exit mitosis. We further showed that the duration of the extended G1 phase varies between cells and can be regulated by changing cyclin D1 and p21 expression, and that the duration of the extended G1 increases gradually, in part by an increase in p21, as cells undergo one or more cell cycles following adipogenic stimulation. In addition, we found that expression of PPARG is repressed during S/G2/M phases and starts to significantly increase only during each extended G1 after mitosis. This rate of PPARG increase after mitosis varies between cells but becomes faster on average the later a mitosis occurs following adipogenic stimulation.

We further showed that PPARG has to reach a critical threshold level before the end of an extended G1 period in order for cells to irreversibly commit to differentiate and close the window of proliferation. However, if a cell is able to reach the end of the extended G1 phase before it reaches the PPARG threshold, the cell will enter the next cell cycle, extend the window of proliferation, and suppress both the increase in PPARG and differentiation until the end of the next mitosis. Thus, our data argues that terminal differentiation occurs out of a probabilistic competition that can occur over one or more cell cycles while the differentiation stimulus is applied.

We further showed that the competition between proliferation and terminal differentiation can be driven by a PPARG-mediated increase in expression of the CDK inhibitor p21 both by PPARG-mediated direct transcriptional induction, and by a FKBPL-mediated increase in p21 half-life. Since p21 has a short-half-life of less than an hour at both the protein and mRNA levels (Yang et al., 2017), this raises a question common to all terminal differentiation processes, how a permanent post-mitotic maintained can be maintained. In adipogenesis, PPARG can function as a continuously active driver since PPARG levels continues to increase and stays high after it reaches the threshold for terminal differentiation independent of the input stimulus, thus both permanently preventing cells from returning to the undifferentiated state as well as permanently driving high p21 levels to maintain the postmitotic state. We show that acute suppressing p21 after cells have passed the threshold for terminal

differentiation re-activates the cell cycle but triggers mitotic defects, arguing that p21 mediates the precise timing between differentiation and terminal cell-cycle exit and that this timing is critical for cell health. Notably, our studies were performed at low cell density, and at higher cell densities the homolog CDK inhibitor p27 likely has a synergistic role along with p21 in regulating the duration of the extended G1. Such a synergistic role of both CDK inhibitors is consistent with knockout data in mice which showed a 6-fold increase in fat mass when p27 and p21 where knocked out together as compared to the individual knockouts (Naaz et al., 2004).

Given that tissues typically have fixed numbers of progenitor cells, our results suggest that organisms can regulate differentiation in two ways. First, by changing the amplitude of adipogenic stimuli, previous studies and our analysis in Figure 7 showed that different percentages of progenitor cells with different sensitivity to adipogenic stimuli can be engaged and end up terminally differentiating (Ahrends et al., 2014; Park et al., 2012). Second, our study here shows that dependent on the duration of the proliferative window, cells stimulated to differentiate do not immediately differentiate but only do so after 1, 2 or 3 cell cycles to generate per progenitor cell 2, 4 or 8 differentiated cells, respectively (Figure 7B). Thus, our study argues that a functional consequence of a system with a regulated proliferative window before terminal differentiation is that organisms can control not only whether or not progenitor cells differentiate but also how many differentiated cells are generated per progenitor cell by having a longer or shorter proliferating window, respectively. A conclusion from our data in Figures 6 and 7 is that the percent of terminally differentiated cells, as well as the duration of the proliferative window and number of differentiated cells produced per progenitor cell, can both be regulated separately over different ranges of mitogen and differentiation stimuli. The large effect of p21 and p27 inhibitor knockouts on fat mass (Naaz et al., 2004), and the role of p21 in regulating the duration of the proliferation window shown here, provide support for the hypothesis that the control of the duration of the proliferative window is a second key mechanism controlling tissue size. Notably, such a role of p21 in adipogenesis may particularly show itself during conditions of stress, DNA damage, and aging that are all associated with increased p21 levels. Finally, the mechanism described

here how cells close the proliferative window requires permanent cell-cycle exit which is likely unique to terminal cell differentiation, since regulatory mechanisms controlling differentiation outcome of pluripotent stem, pancreatic beta or other cells that only temporarily slow proliferation during differentiation are likely different.

METHODS

Generation of PPARG/geminin dual-reporter cell line.

OP9 cells with endogenously tagged citrine-PPARG2 and stably infected H2B-mTurqoise was generated as previously(Bahrami-Nejad et al., 2018). Lentivirus was generated for the geminin degron reporter from the vector pCSII-EF-Geminin(1-110)-mCherry. A third-generation lentiviral packaging system was used and consisted of the following packaging vectors: pMDlg, pCMV-VSVG, and pRSV-Rev. The geminin reporter was then stably infected into H2B-mTurqoise/citrine-PPARG2 cells to generate the dual-reporter cell lines. Selection of dual-reporter cells was done with FACS for mCherry-positive cells.

Generation of a PPARG/geminin/CDK2 triple reporter cell line.

Lentivirus was generated for the CDK2 sensor from the vector pCSII-EF-DHB-mTurquoise (gift from the lab of Tobias Meyer) in the same manner described above and used to infect the dual reporter PPARG/geminin cells. Selection of triple-reporter cells was done with FACS for cells that were positive for both mCherry and mTurquoise.

Generation of a PPARG/CRL4-CDT reporter cell line.

The CRL4-Cdt2 construct was developed by Atsushi Miyawaki's lab (Sakaue-Sawano et al., 2017) and was obtained from the lab of Tobias Meyer. We changed the fluorescent tag to iRFP670 and generated lentivirus in the same manner described above. Selection of triple-reporter cells stably expressing iRFP670-CRL4-Cdt2 was done with FACS for cells that were positive for both mCherry and iRFP670.

Cell culture and differentiation.

Wildtype and reporter OP9 cell lines were cultured according to previously published protocols (Ahrends et al., 2014; Bahrami-Nejad et al., 2018; Wolins et al., 2006). Briefly, the cells were cultured in growth media consisting of MEM-α media (ThermoFisher Scientific) containing 100 units/mL Penicillin, 100mg/mL Streptomycin, and 292 mg/mL L-glutamate supplemented with 20% FBS. To induce differentiation, two methods were used. In the first method, a standard DMI cocktail was used: cells were treated with 125 μM IBMX (Sigma-Aldrich), 1 μM dexamethasone (Sigma-Aldrich), and 1.75 nM insulin (Sigma-Aldrich) for 48h, followed by 1.75 nM insulin for 48h. In the second method, cells were treated with 1 μM of Rosiglitazone (Cayman, USA) for 48 hours, followed by 1.75 nM insulin for another 48 hours. For fixed cell experiments, the differentiation stimuli were added to the growth media described above with one modification: 10% FBS was used (instead of 20% FBS) during differentiation

conditions. The one exception is in in the reduced serum experiments in Figure 4D, in which 2% FBS was used in the growth media during differentiation. For all live cell experiments, the differentiation stimuli were added to Fluorobrite DMEM media (ThermoFisher Scientific) containing 100 units/mL Penicillin, 100mg/mL Streptomycin, and 292 mg/mL L-glutamate supplemented with 10% FBS. For Figure 4D, EGF (Sigma-Aldrich E9644) was used at a final concentration of 1 μg/mL, and a MEK inhibitor PD0325091 was used at a final concentration of 100 nM.

siRNA-mediated gene silencing.

siRNA targeting *Pparg, Cebpa, p21, CyclinD1, Fkbpl* and the AllStars Negative Control siRNA were purchased from QIAGEN. For siRNA knockdown in the live-cell imaging experiments in dual-reporter cells (Figure 4, Figures 5a, 5d, and 5e), OP9 cells were transfected by reverse-transfection using μL Lipofectamine RNAiMax (Invitrogen). Briefly, our reverse-transfection protocol per well is as follows: mixed 20 μL of Optimem, 0.5 μL of a 10 μM siRNA stock solution, and 0.3 μL of RNAiMax. Let solution incubate at room temperature for 10 minutes and then add 80 μL of culture media containing the desired number of cells per well. Then the entire (~100μL) volume is plated into one well of a 96-well plate. The siRNA/RNAiMax mixture was left on the cells for 24 hours before being aspirated away and replaced with fresh culture media containing DMI to begin the differentiation protocol.

For the live-cell imaging experiments in dual-reporter cells transfected at the 48-hour timepoint (Figure 6), the following protocol per well was used: siRNA mixture was prepared using 0.6 μL Lipofectamine RNAiMAX, 0.5 μL of a 10 μM siRNA stock solution, and 20 μL of Optimem. Incubate the mixture for 10 minutes then add 180 μL of Fluorobrite media consisting of 1.75 nM insulin. The entire solution (~200μL total volume) was then added to cells at the 48-hour time point and left on until the end of the experiment.

Overexpression of p21

A retroviral vector containing DHFR-Chy-p21(Spencer et al., 2013) (gift from the lab of Tobias Meyer) was used to generate viral particles to stably infect DHFR-Chy-p21into a modified dual-reporter cell line. This cell line was also stably infected with H2B-iRFP670 and a version of the geminin degron fused to mCerulean3. Positive clones were selected for by FACS in cell culture media containing 10 μM TMP. Cells were sorted into culture media with no TMP and grown in the absence of TMP. All overexpression experiments were done by adding 10 μM TMP into the culture media or differentiation media. In control experiments, 10 μM DMSO was added instead of TMP.

Immunofluorescence (IF) staining

All cultured cells were fixed with 4% PFA in PBS for 30 min at room temperature, followed by five washes with PBS using an automated plate washer (Biotek). Cells were then permeabilized with 0.1% Triton X-100 in PBS for 15 minutes at 4°C, followed by blocking for 1 hour in 5% bovine serum albumin (BSA, Sigma Aldrich) in PBS. The cells were incubated with primary antibodies in 2% BSA in PBS overnight at 4°C: mouse anti-PPARγ (Santa Cruz Biotech, sc-7273, 1:1,000), rabbit anti-CEBPα (Santa Cruz Biotech, sc-61, 1:1,000), mouse anti-p21 (Santa Cruz Biotech, sc-6246, 1:100), cyclinD1 (Abcam, ab137145,1:1,000), adiponectin (Abcam, ab22554, 1:1,000), Glut4 (Santa Cruz Biotech, sc-1608,1:500), FABP4 (R&D Systems, AF1443, 1:1,000). After washing, cells were incubated with Hoechst (1:20,000) and secondary antibodies in 2% BSA / PBS for 1 hour. Secondary antibodies included AlexaFluor-conjugated anti-rabbit, anti-mouse , and anti-goat antibodies (Thermo Fisher Scientific). All secondary antibodies were used at a 1:1,000 dilution. Where indicated, lipids were co-stained by adding HCS LipidTOX Deep Red Neutral Lipid Stain 637/655 (1:1,000), ThermoFisher Scientific H34477) to secondary antibody solution. Cells were washed five times with PBS in an automated plate washer prior to imaging. For fixed-cell timecourse experiments, approximately 7,000 wildtype or dual-reporter OP9 cells were used to calculate mean values at each timepoint for each technical replicate.

RNAseq

siRNA targeting Pparg (# L-040712-00-0005) and Negative Control siRNA (# D-001810-10-05) were purchased from Dharmacon and transfected into OP9 cells using Lipofectamine RNAiMax (Invitrogen) according to the manufacturer's protocol. siRNA was used at a concentration of 25 nM, and the RNAiMAX/siRNA mixture was applied for 48 hours prior to the induction of differentiation. For gene expression analysis of OP9 cell samples, the cells were differentiated for 144 hours using a previously described protocol(Ahrends et al., 2014). RNA from three independent biological experiments were collected at different time points before and after induction of differentiation including (d0-d6) the extraction was completed using RNeasy Mini Kit (QIAGEN, Cat. 74104). RNA quality of all samples (n=7 time points and n=3 experiments from independent passages) was evaluated by both Nanodrop for (A260/280 >2) and Bioanalyzer 2100 High Sensitivity RNA Analysis chips (Agilent, Cat. 5067-1513) which displayed intact RNA integrity (RIN >9). mRNA samples were concentrated to ≤ 5 μl by MinElute column (QIAGEN, Cat. 74204). For generation of RNA-seq libraries, polyadenylated mRNA was isolated from 300 ng of total RNA by incubation with oligo-DT attached magnetic beads and followed by strand-specific library preparation using the TruSeq Stranded mRNA Library Preparation kit (Ilumina, Cat. 20020595). Briefly, isolated polyadenylated mRNA was fragmented using divalent cations under elevated temperature and 1st and 2nd strands DNA were synthesized using SuperScript

II Reverse Transcriptase (provided with Ilumina kit). A-tailing and adapter ligation was performed according to the manufacturer's protocol; the resulting dsDNA was enriched in a PCR reaction based on predetermined CT values and cleaned using AMPure XP beads (provided with Ilumina kit). Concentrations of enriched dsDNA fragments with specific adapters were determined and base pair average size as well as library integrity were analyzed using the Bioanalyzer DNA High Sensitivity chips (Agilent, Cat. 5067-4626). Samples were pooled and sequenced on the Illumina NextSeq 500/550 High Output platform (Illumina, FC-404-2002) up to 18 samples per lane with 1% PhiX spike as a control.

The read quality of the raw FASTQ files was checked with FastQC(Andrews and Babraham Bioinformatics, 2010) (v0.11.7). Next, reads were pseudo-aligned to the mouse reference transcriptome (Mus_musculus.GRCm38.cdna) using Kallisto(Bray et al., 2016) (v0.44.0) with the quantification algorithm enabled, the number of bootstraps set to 100, and run in paired-end mode. The Kallisto output files were read into R using Sleuth, and the transcripts per million (TPM), a measurement of the proportion of transcripts in the RNA pool, was used for downstream differential expression analysis(Pimentel et al., 2017).

ChiP experiments

ChIP was performed essentially as described previously (Siersbaek et al., 2014). Briefly, ChIP was performed on 10 min %1 formaldehyde crosslinked chromatin, and two biological experiments were used. Cross-linking was stopped by the addition of glycine to a final concentration of 0.125 M for 10 min, followed by addition of ChIP lysis buffer (1% Triton X-100, 0.1% SDS, 150 mM NaCl, 1 mM EDTA, and 20 mM Tris, pH 8.0). Samples were sonicated using the Diagenode Bioruptor 300 (4 X 8 cycles, 30 s on/off, maximum level). Samples were centrifuged for 1 min at 10,000 X g, the fat layer was removed, and the supernatant was used for subsequent chromatin IP using PPARG (E-8, sc-7273 X; Santa Cruz) and IgG (sc-2025; Santa Cruz). For single IPs, chromatin from 1,000,000 cells was used. Following 3 h rotation at 4°C, 50 μl protein A Sepharose Fast Flow beads (GE Healthcare Life Sciences) was added and samples were incubated overnight at 4°C with rotation. Beads were washed at 4°C once with IP wash buffer 1 (1% Triton, 0.1% SDS, 150 mM NaCl, 1 mM EDTA, 20 mM Tris, pH 8.0, and 0.1% sodium deoxycholate [NaDOC]), twice with IP wash buffer 2 (1% Triton, 0.1% SDS, 500 mM NaCl, 1 mM EDTA, 20 mM Tris, pH 8.0, and 0.1% NaDOC), once with IP wash buffer 3 (0.25 M LiCl, 0.5% NP-40, 1 mM EDTA, 20 mM Tris, pH 8.0, and 0.5% NaDOC), and finally twice with IP wash buffer 4 (10 mM EDTA and 200 mM Tris, pH 8), all at 4°C. DNA-protein complexes were eluted with 400 μl of elution buffer (1% SDS and 0.1 M NaHCO3) and de-cross-linked by adding NaCl to a final

concentration of 0.2 M and shaking for 3 h at 65°C. ChIPed DNA was purified using phenol-chloroform and analyzed by qPCR.

ChIP-qPCR primer	Forward Sequence	Reverse Sequence
Arbp/36b4	CTGGGACGATGAATGAGGAT	AGCAGCTGGCACCTAAACAG
insulin	CTTCAGCCCAGTTGACCAAT	AGGGAGGAGGAAAGCAGAAC
aP2	AATGTCAGGCATCTGGGAAC	GACAAAGGCAGAAATGCACA
Pdk4	GGATTTCAACAGCCAGTGCT	ATAGTGCTGCCCAGTGTGTG
P21_1	AATTGGAGTCAGGCGCAGAT	GCATTGCTACGGGGAAGAAC
P21_2	GTGGCTGAAGGCTTCGTTTG	CATCCGTGGTCCTGGAGTTC
P21_3	TTTGTTGTCCTCGCCCTCAT	CTCCACCTTGATCTCCACGC

Measuring protein decay rates using cycloheximide

Protein decay rates were quantified as previously described(Bahrami-Nejad et al., 2018). Briefly 10,000 OP9 cells were seeded in 96-well plates) one plate for each timepoint. Cells were induced to differentiate with DMI for 24 hours. Cyclohexamide was added to the media at a final concentration of 30 μM. Cells were fixed and stained at different times after addition of cyclohexamide, and immunofluorescence was used to quantify protein concentration. Half-lives were obtained by fitting first order exponential decay curves to the data.

Fluorescent imaging

Imaging was conducted using an ImageXpress MicroXL (Molecular Devices, USA) with a 10X Plan Apo 0.45 NA objective. Live fluorescent imaging was conducted at 37°C with 5% CO_2. A camera bin of 2x2 was used for all imaging condition. Cells were plated in optically clear 96-well plates: plastic-bottom Costar plates (#3904) for fixed imaging or Ibidi μ-Plate (#89626) for live imaging. Living cells were imaged in FluoroBrite DMEM media (Invitrogen) with 10% FBS, 1% Penicillin/Streptomycin and insulin to reduce background fluorescence. Images were taken every 12 min in different fluorescent channels: CFP, YFP and/or RFP. Total light exposure time was kept less than 700 ms for each time point. Four, non-overlapping sites in each well were imaged. Cell culture media were changed at least every 48h.

Imaging data processing

Data processing of fluorescent images was conducted in MATLAB R2016a (MathWorks). Unless stated otherwise, fluorescent imaging data were obtained by automated image segmentation, tracking and measurement using the MACKtrack package for MATLAB. Quantification of PPARG- and CEBPA-positive cells in fixed samples was based on quantification of mean fluorescence signal over nuclei.

Cells were scored as PPARG- and CEBPA-positive if the marker expression level was above a preset cut-off determined by the bimodal expression at the end of the experiment.

For live imaging data of OP9 cells, the CFP channel capturing H2B-mTurqoise fluorescence was used for nuclear segmentation and cell tracking. Obtained single-cell traces were filtered to removed incomplete or mistracked traces according to the following criteria: cells absent within 6 hours of the endpoint, cell traces that started more than 4 hours after the first timepoint, cells that had large increase or decrease in PPARG intensity normalized to the previous timepoint, cells where H2B drops did not match drops in the geminin sensor. If cells were binned according to their PPARG expression, cells were binned based on their mean nuclear PPARG expression at the described timepoints.

The percent of cells in the S/G2/M phases at each time point is calculated by counting the cells that expressed the geminin reporter during the 96-hour differentiation period divided by the total number of cells. The percent of PPARG high cells was assessed by counting cells that above the PPARG threshold at that time point and dividing by the total number of cells at that time point.

Estimating a differentiation commitment point

PPARG values at the end of a differentiation experiment typically exhibit a bimodal distribution. In order to estimate a commitment point, PPARG values at the last frame of the experiment was fit to a 2 component gaussian mixture model. Cells were then classified as either differentiated or undifferentiated based on whether they more closely associated with the high or low component of the mixture model, respectively. The commitment point was then assessed as the value of PPARG at the 48-hour time point, before the stimuli was removed, that predicted the final differentiation classification with a false positive rate of less that 5%. In experiments where multiple conditions are present, the gaussian mixture model was only fitted to the negative control and the commitment point was selected based on the negative control model and applied to all other conditions in the same experiment.

Statistics

Unless specified otherwise, data are expressed as mean +/- standard error of the mean (S.E.M). Live traces are expressed as median +/- interquartile range (25th-75th percentiles). For histograms with a y-axis labeled “Fraction of Cells,” each histogram (not each plot) is normalized to the total number of cells in the population of that histogram such that all bars in the histogram add to 1. Representative results are representative of at least two independent experiments.

Data availability

All relevant data from this manuscript are available upon request.

REFERENCES

Ahrends, R., Ota, A., Kovary, K.M., Kudo, T., Park, B.O., and Teruel, M.N. (2014). Controlling low rates of cell differentiation through noise and ultrahigh feedback. Science *344*, 1384–1389.

Andrews, S., and Babraham Bioinformatics (2010). FastQC: A quality control tool for high throughput sequence data. Manual doi:citeulike-article-id:11583827.

Bahrami-Nejad, Z., Zhao, M.L., Tholen, S., Hunerdosse, D., Tkach, K.E., van Schie, S., Chung, M., and Teruel, M.N. (2018). A Transcriptional Circuit Filters Oscillating Circadian Hormonal Inputs to Regulate Fat Cell Differentiation. Cell Metab. *27*, 854-868.e8.

Blais, A., Tsikitis, M., Acosta-Alvear, D., Sharan, R., Kluger, Y., and Dynlacht, B.D. (2005). An initial blueprint for myogenic differentiation. Genes Dev. *19*, 553–569.

Bray, N.L., Pimentel, H., Melsted, P., and Pachter, L. (2016). Near-optimal probabilistic RNA-seq quantification. Nat. Biotechnol. *34*, 525–527.

Buttitta, L.A., and Edgar, B.A. (2007). Mechanisms controlling cell cycle exit upon terminal differentiation. Curr. Opin. Cell Biol. *19*, 697–704.

Buttitta, L.A., Katzaroff, A.J., Perez, C.L., de la Cruz, A., and Edgar, B.A. (2007). A Double-Assurance Mechanism Controls Cell Cycle Exit upon Terminal Differentiation in Drosophila. Dev. Cell *12*, 631–643.

Calder, A., Roth-Albin, I., Bhatia, S., Pilquil, C., Lee, J.H., Bhatia, M., Levadoux-Martin, M., McNicol, J., Russell, J., Collins, T., et al. (2012). Lengthened G1 Phase Indicates Differentiation Status in Human Embryonic Stem Cells. Stem Cells Dev. *22*, 279–295.

Cappell, S.D., Chung, M., Jaimovich, A., Spencer, S.L., and Meyer, T. (2016). Irreversible APCCdh1 Inactivation Underlies the Point of No Return for Cell-Cycle Entry. Cell *166*, 167–180.

Farmer, S.R. (2006). Transcriptional control of adipocyte formation. Cell Metab. *4*, 263–273.

Fu, M., Rao, M., Bouras, T., Wang, C., Wu, K., Zhang, X., Li, Z., Yao, T.P., and Pestell, R.G. (2005). Cyclin D1 inhibits peroxisome proliferator-activated receptor γ-mediated adipogenesis through histone deacetylase recruitment. J. Biol. Chem. *280*, 16934–16941.

Ghaben, A.L., and Scherer, P.E. (2019). Adipogenesis and metabolic health. Nat. Rev. Mol. Cell Biol. *20*, 242–258.

Grant, G.D., Kedziora, K.M., Limas, J.C., Cook, J.G., and Purvis, J.E. (2018). Accurate delineation of cell cycle phase transitions in living cells with PIP-FUCCI. Cell Cycle *17*, 2496–2516.

Guo, K., Wang, J., Andrés, V., Smith, R.C., and Walsh, K. (1995). MyoD-induced expression of p21 inhibits cyclin-dependent kinase activity upon myocyte terminal differentiation. Mol. Cell. Biol. *15*, 3823–3829.

Halevy, O., Novitch, B.G., Spicer, D.B., Skapek, S.X., Rhee, J., Hannon, G.J., Beach, D., and Lassar, A.B. (1995). Correlation of terminal cell cycle arrest of skeletal muscle with induction of p21 by MyoD. Science *267*, 1018–1021.

Han, S., Sidell, N., FIsher, P., and Roman, J. (2004). Up-regulation of p21 Gene Expression by Peroxisome Proliferator-Activated Receptor in Human Lung Carcinoma Cells. Clin. Cancer Res. *10*, 1911–1919.

Hardwick, L.J.A., Ali, F.R., Azzarelli, R., and Philpott, A. (2015). Cell cycle regulation of proliferation versus differentiation in the central nervous system. Cell Tissue Res. *359*, 187–200.

Jascur, T., Brickner, H., Salles-Passador, I., Barbier, V., El Khissiin, A., Smith, B., Fotedar, R., and Fotedar, A. (2005). Regulation of p21WAF1/CIP1 Stability by WISp39, a Hsp90 Binding TPR Protein. Mol. Cell *17*, 237–249.

Jeffery, E., Church, C.D., Holtrup, B., Colman, L., and Rodeheffer, M.S. (2015). Rapid depot-specific activation of adipocyte precursor cells at the onset of obesity. Nat. Cell Biol. *17*, 376–385.

Jones, P.H., Simons, B.D., and Watt, F.M. (2007). Sic Transit Gloria: Farewell to the Epidermal Transit Amplifying Cell? Cell Stem Cell *1*, 371–381.

Krentz, N.A.J., van Hoof, D., Li, Z., Watanabe, A., Tang, M., Nian, C., German, M.S., and Lynn, F.C. (2017). Phosphorylation of NEUROG3 Links Endocrine Differentiation to the Cell Cycle in Pancreatic Progenitors. Dev. Cell *41*, 129-142.e6.

Lacomme, M., Liaubet, L., Pituello, F., and Bel-Vialar, S. (2012). NEUROG2 Drives Cell Cycle Exit of Neuronal Precursors by Specifically Repressing a Subset of Cyclins Acting at the G1 and S Phases of the Cell Cycle. Mol. Cell. Biol. *32*, 2596–2607.

Lange, C., Huttner, W.B., and Calegari, F. (2009). Cdk4/CyclinD1 Overexpression in Neural Stem Cells Shortens G1, Delays Neurogenesis, and Promotes the Generation and Expansion of Basal Progenitors. Cell Stem Cell *5*, 320–331.
Liu, L., Michowski, W., Kolodziejczyk, A., and Sicinski, P. (2019). The cell cycle in stem cell proliferation, pluripotency and differentiation. Nat. Cell Biol. *21*, 1060–1067.
Matson, J.P., Dumitru, R., Coryell, P., Baxley, R.M., Chen, W., Twaroski, K., Webber, B.R., Tolar, J., Bielinsky, A.K., Purvis, J.E., et al. (2017). Rapid DNA replication origin licensing protects stem cell pluripotency. Elife *6*, 1–31.
Miyatsuka, T., Kosaka, Y., Kim, H., and German, M.S. (2011). Neurogenin3 inhibits proliferation in endocrine progenitors by inducing Cdkn1a. Proc. Natl. Acad. Sci. U. S. A. *108*, 185–190.
Naaz, A., Holsberger, D.R., Iwamoto, G.A., Nelson, A., Kiyokawa, H., and Cooke, P.S. (2004). Loss of cyclin-dependent kinase inhibitors produces adipocyte hyperplasia and obesity. FASEB J. *15*, 1–15.
Park, B.O., Ahrends, R., and Teruel, M.N. (2012). Consecutive positive feedback loops create a bistable switch that controls preadipocyte-to-adipocyte conversion. Cell Rep. *2*, 976–990.
Parker, S., Eichele, G., Zhang, P., Rawls, A., Sands, A., Bradley, A., Olson, E., Harper, J., Elledge, S., Rawls, A., et al. (2006). p53-independent expression of p21Cip1 in muscle and other terminally differentiating cells. Science *267*, 1024–1027.
Pauklin, S., and Vallier, L. (2013). The cell cycle state of stem cells determines cell fate propensity. Cell *155*, 135–147.
Pimentel, H., Bray, N.L., Puente, S., Melsted, P., and Pachter, L. (2017). Differential analysis of RNA-seq incorporating quantification uncertainty. Nat. Methods *14*, 687–690.
Qiu, Z., Wei, Y., Chen, N., Jiang, M., Wu, J., and Liao, K. (2001). DNA Synthesis and Mitotic Clonal Expansion Is Not a Required Step for 3T3-L1 Preadipocyte Differentiation into Adipocytes. J. Biol. Chem. *276*, 11988–11995.
Rosen, E.D., and Spiegelman, B.M. (2014). What we talk about when we talk about fat. Cell *156*, 20–44.
Ruijtenberg, S., and van den Heuvel, S. (2016). Coordinating cell proliferation and differentiation: Antagonism between cell cycle regulators and cell type-specific gene expression. Cell Cycle *15*, 196–212.
Ruijtenberg, S., van den Heuvel, S., and Van Den Heuvel, S. (2015). G1/S Inhibitors and the SWI/SNF Complex Control Cell-Cycle Exit during Muscle Differentiation. Cell *162*, 300–313.
Sakaue-Sawano, A., Kurokawa, H., Morimura, T., Hanyu, A., Hama, H., Osawa, H., Kashiwagi, S., Fukami, K., Miyata, T., Miyoshi, H., et al. (2008). Visualizing spatiotemporal dynamics of multicellular cell-cycle progression. Cell *132*, 487–498.
Sakaue-Sawano, A., Yo, M., Komatsu, N., Hiratsuka, T., Kogure, T., Hoshida, T., Goshima, N., Matsuda, M., Miyoshi, H., and Miyawaki, A. (2017). Genetically Encoded Tools for Optical Dissection of the Mammalian Cell Cycle. Mol. Cell *68*, 626-640.e5.
Siersbaek, R., Rabiee, A., Nielsen, R., Sidoli, S., Traynor, S., Loft, A., Poulsen, L., Rogowska-Wrzesinska, A., Jensen, O.N., and Mandrup, S. (2014). Transcription factor cooperativity in early adipogenic hotspots and super-enhancers. Cell Rep. *7*, 1443–1455.
Soufi, A., and Dalton, S. (2016). Cycling through developmental decisions : how cell cycle dynamics control pluripotency , differentiation and reprogramming. Development 4301–4311.
Spencer, S.L., Cappell, S.D., Tsai, F.C., Overton, K.W., Wang, C.L., and Meyer, T. (2013). The proliferation-quiescence decision is controlled by a bifurcation in CDK2 activity at mitotic exit. Cell *155*, 369–383.
Tang, Q., Otto, T.C., and Lane, M.D. (2003). Mitotic clonal expansion: a synchronous process required for adipogenesis. Proc. Natl. Acad. Sci. U. S. A. *100*, 44–49.
Wolins, N.E., Quaynor, B.K., Skinner, J.R., Tzekov, A., Park, C., Choi, K., and Bickel, P.E. (2006). OP9 mouse stromal cells rapidly differentiate into adipocytes: characterization of a useful new model of adipogenesis. J. Lipid Res. *47*, 450–460.
Wu, Z., Rosen, E.D., Brun, R., Hauser, S., Adelmant, G., Troy, A.E., McKeon, C., Darlington, G.J., and Spiegelman, B.M. (1999). Cross-Regulation of C/EBPα and PPARγ Controls the Transcriptional Pathway of Adipogenesis and Insulin Sensitivity. Mol. Cell *3*, 151–158.
Yang, H.W., Chung, M., Kudo, T., and Meyer, T. (2017). Competing memories of mitogen and p53 signalling control cell-cycle entry. Nature *549*, 404–408.

Zalc, A., Hayashi, S., Auradé, F., Bröhl, D., Chang, T., Mademtzoglou, D., Mourikis, P., Yao, Z., Cao, Y., Birchmeier, C., et al. (2014). Antagonistic regulation of p57 kip2 by Hes/Hey downstream of Notch signaling and muscle regulatory factors regulates skeletal muscle growth arrest. Development *141*, 2780–2790.

AUTHOR CONTRIBUTIONS

M.L.Z. and M.N.T. conceived experiments. M.L.Z., K.K., A.R., and Z.B. performed experiments and analyzed data. M.L.Z. and B.T. wrote the image analysis scripts. M.L.Z. and M.N.T wrote the paper with input from all authors.

ACKNOWLEDGEMENTS

This work was supported by National Institutes of Health RO1-DK101743, RO1-DK106241, P50-GM107615, a Stanford BioX Seed Grant, and a Stanford Diabetes Research Center Seed Grant (to M.N.T.), NIH F32 Postdoctoral Fellowship 5F32DK114981-02 (to B.T.), and T32-NIH T2HG00044 and NIH F31 Predoctoral Fellowship 1F31DK112570-01A1 (to M.L.Z.). The authors would like to thank Tobias Meyer, Takamasu Kudo, Antoine Zalc, Lindsey Pack (Stanford), Steve Cappell (NIH), and members of Teruel lab for helpful discussions and critical reading of the manuscript.

FIGURE LEGENDS

Figure 1. Measurement of the precise time when cells irreversibly commit to differentiate based on live single-cell analysis of endogenous expression levels of PPARG.

(A) Images of cells expressing endogenous citrine-PPARG that were differentiated using the standard 96-hour DMI protocol. Scale bar, 50 μm.

(B) Results of a typical experiment in which thousands of single cells were stimulated to differentiate. Thirty single-cell traces are shown as examples. Representative of 4 independent experiments.

(C) Scatter plot using data from (B) showing PPARG levels for each cell at 48 hours, just before the DMI stimulus was removed, and at 96 hours. Dashed black line represents the PPARG threshold (see Methods). Cells were defined as differentiated (blue) or undifferentiated (orange) by whether their PPARG levels were in the high or low intensity distributions, respectively.

(D) Citrine-PPARG cells were differentiated using the DMI protocol, and immunocytochemistry was performed at 96 hours for adipocyte markers (for each scatter plot: n > 4000 cells, representative of 2 independent experiments).

(E) The timecourses from (B) were split into equal-width bins by their PPARG values at 0, 24, 48, and 72 hours. The fraction of differentiated cells represents the number cells that crossed the PPARG threshold at the end of the experiment divided by the number of cells in the bin.

(F) Differentiating cells from (B) were computationally aligned so that the zero timepoint represents the time when the cell crossed the PPARG threshold. Plot shows 5 representative single cell traces, the median (solid black line), and the 5th-95th percentile (shaded region).

(G) PPARG timecourses from the cells that differentiated after 96 hours in (D) were computationally aligned as in (F) and plotted (blue curves). At each aligned time point, the Pearson correlation coefficient between the aligned PPARG values and the endpoint immunofluorescence values for adipocyte markers was calculated (red curves). As a comparison, PPARG values for the Glut4 panel were aligned to a randomized PPARG threshold crossing point. The randomized crossing point was generated by scrambling the vector of measured threshold points for each cell so that each threshold point is matched with different cell.

(B-F) The dotted line represents the calculated PPARG threshold for that experiment.

Figure 2. Development of a system to measure timecourses of cell cycle phases and terminal cell differentiation dynamics simultaneously in thousands of individual cells.

(A) Dual reporter cells were made by stably expressing H2B-mTurquoise(CFP) and geminin-degron-mCherry(RFP). Data from a representative single cell entering the cell cycle is shown. Anaphase is shown both by a split in the H2B-mTurquoise signal (top images) and by a sharp drop in geminin signal (bottom timecourse). Scale bar, 20 μm. White outlines mark the position of nuclei in cells after anaphase. To validate that the geminin degron sensor is suitable to monitor G1 length in the OP9 preadipocyte cell system, we compared its dynamics to that of a reporter of CRL4-Cdt2-mediated degradation that provides a more precise measure of the G1/S transition (Grant et al., 2018; Sakaue-Sawano et al., 2017) and confirmed that the dynamics of the two reporters are closely correlated (Figure S2).

(B) The dual reporter cells allow simultaneous measurement in thousands of single cells of differentiation state using PPARG levels (left) and cell cycle state using the geminin-degron sensor (right). The timepoints at which mitosis occurred were determined by using the split in H2B signal

(black open circles). Representative of 4 independent experiments.
(C) Comparison of the number of observed mitotic events that occurred in cells that were differentiated versus cells that remained undifferentiate at the end of the 96-hour experiment shown in (B).
(D) Plot showing how the fraction of cells in S/G2/M (red) or with PPARG levels higher than the threshold (blue) varies during a 96-hour differentiation timecourse induced by DMI.
(E) Examples of PPARG (blue) and geminin-degron (red) timecourses obtained in the same single cell. Cells were stimulated to differentiate with DMI using the standard adipogenic protocol. The yellow dot in each plot marks the time at which that cell reached the PPARG threshold and irreversibly committed to the differentiated state.
(F) Histogram of the difference between the time when the PPARG threshold is crossed and when mitosis last occurred for each cell in the experiment shown in (B). The PPARG threshold is reached on average ~14 hours after the last mitosis is completed. Median value is 11 hours. Negative values indicate cells that reached the PPARG threshold before the last mitosis was completed.

Figure 3. PPARG controls cell cycle activity in part by upregulating p21 expression.
(A-D) Application of the standard DMI cocktail for 48 hours was used to induce differentiation.
(A) Dual-reporter cells were transfected with PPARG or control siRNA and then stimulated to differentiate. The percent of cells in S/G2/M phases at each time point is calculated by counting the cells that expressed the geminin reporter during the 96-hour differentiation period divided by the total number of cells. The percent of PPARG high cells was assessed by counting the cells with PPARG levels above the threshold divided by the total number of cells at the respective timepoint. Cells were induced to differentiate with the standard DMI protocol. Approximately 5000 cells were analyzed per experiment. Representative of 3 independent experiments.
(B) Wildtype OP9 cells were transfected with PPARG or nontargeting siRNA and then stimulated to differentiate. RNA samples were collected every 24 hours for 144 hours. Data is plotted as transcripts per million (TPM), and mean ± 1 SD is shown for three replicates.
(C) Dual-reporter cells were transfected with p21, p18, or nontargeting siRNAs and stimulated to differentiate. The number of cell divisions per cell is reported in the normalized histograms. Representative of 2 independent experiments.
(D) Wildtype OP9 cells were stimulated with rosiglitazone for 48 hours. Chromatin immunoprecipitation (ChIP) of PPARG was performed followed by qPCR. Three sites on the p21 promoter are shown. The promoters of insulin and Arbp/36b4 served as negative controls, and known PPARG target genes Fabp4/aP2 and Pdk4 (pyruvate dehydrogenase kinase, isoenzyme 4) were used as positive controls. Data are normalized to a nontarget genomic site and IgG enrichment. Two biological experiments were used. Two-way ANOVA with Bonferroni's multiple comparisons test was applied for statistical analysis. Values represent means ± SEM. $p<0.05$, ** $p<0.01$, *** $p<0.001$, **** $p<0.0001$.
(E) Wildtype OP9 cells were stimulated to differentiate by addition of 1 μM rosiglitazone. p21 levels were measured by fixing and staining cells at subsequent times. Approximately 5000 cells were analyzed per experiment. Data is plotted as mean (line) along with the values for each of the three experiments (points).
(F) Wildtype OP9 cells were transfected with p21 or Control siRNA and stimulated to differentiate by addition of 1 μM rosiglitazone. Differentiation and cell cycle progression were assessed in the same manner as in Figure 3A.
(G) FKBPL expression under nontargeting vs PPARG knockdown were obtained from the RNA-seq

data in (B). Data reported as TPM, mean ± 1 SD.
(H) Wildtype OP9 cells were transfected with FKBPL or nontargeting siRNAs, and DMI was added to initiate differentiation. Stability of p21 and PPARG were assessed by adding 30 μM cycloheximide to the media 24 hours after DMI addition and then fixing and staining for protein levels at different subsequent times. Approximately 5000 cells were analyzed per experiment. Data is plotted as mean ± 1 SD of three replicates.

Figure 4. Cells crossing the PPARG threshold for differentiation become unresponsive to mitogenic stimulation and are locked into a post-mitotic state by p21.
(A) Citrine-PPARG and geminin levels were measured in dual-reporter cells in response to media replacement at 48 hours. Cells were separated into ten bins based on their PPARG levels at 48 hours. Plotted lines show mean values for each bin. Inset shows the geminin-degron signal between 48-96 hours. Representative of 2 independent experiments.
(B) PPARG values before serum refresh were binned from 100 to 2500 a.u. in 100 a.u. increments. The plot shows for each bin the fraction of cells with a minimum of one division (measured by a split in nuclear H2B signal, red) and the final p21 level (black) and in response to serum refresh. The histogram shows the number of cells in each bin. The dotted black line shows the PPARG threshold for this experiment. Data from experiment in (A).
(C) PPARG, CEBPA, p21, and nontargeting siRNA were transfected into the dual-reporter cells at 48 hours after DMI addition. siRNA knockdown efficiency is shown in Figure S5. Representative of 3 independent experiments.
(D) A similar analysis as described in (A) was performed on the nontargeting and p21 knockdown conditions from (C).
(E) Left, A similar analysis as in (B) was performed on the nontargeting and p21 knockout conditions from (D). Right, the same data normalized to the first PPARG bin.
(F) Images of control and p21-knockdown cells from (C) obtained 48 hours after siRNA transfection (at 96 hours). Red arrows indicate representative multi-nucleated cells. Scale bar, 50 μm.
(G) OP9 cells were induced to differentiate with rosiglitazone. Cyclin D1, p21 and PPARG levels were assessed by immunocytochemistry. The PPARG threshold for the whole experiment (dotted black line) was calculated at the end of the 96-hour differentiation protocol. Representative of 2 independent experiments.

Figure 5. Adipogenic stimuli initiate a competition between proliferation and differentiation during a gradually extending G1 phase.
(A) Comparison of the time to commit to the next cell cycle (marked by upregulation of geminin) versus time to commit to differentiation in cells that underwent 2-3 mitoses before differentiating. Right, Schematic showing that the end of the second-to-last mitosis is used as the starting reference time for each cell. Left, histograms comparing the two times measured in the same cell (data from Figure 2B, n > 4000 cells, representative of 4 replicates).
(B) Left, Schematic showing which G1-periods were compared. Right, Histograms of the durations of the 1st and 2nd G1-periods in cells from (A) that have undergone at least 3 divisions.See also Figure SXX.
(C) Differentiated cells from (A) were separated into three groups based on when they last exited mitosis. The traces were aligned by the last mitosis frame. The median PPARG levels were plotted for each group (dark line). Shaded region represents the 95th confidence interval.
(D) Timecourses from (A) were categorized into 9 bins based on time of last mitosis. The geminin peak

for each bin is plotted to illustrate when the last mitosis occurred relative to addition of the adipogenic (DMI) stimulus.
(E) Left, Plot showing the average time of the last mitosis versus the average time it took for cells in that bin to increase PPARG levels to the differentiation commitment point. Right, Plot of binned cells from (E) showing the average time spent in G1 versus the percent of cells in that bin that were PPARG high.
(F) Schematic of the three stages of G1-extension, in response to an adipogenic (DMI) stimulus. During the intermediate phase of G1-extension, stochastic competition between proliferation and differentiation causes cells to probabilistically exit into a differentiated or proliferating state. This phase defines how many differentiated cells are generated on average from a precursor cell.

Figure 6. Regulation of G1 duration oppositely controls the percent versus the total number of terminally differentiated cells.
(A) Dual-reporter cells were transfected with p21 or nontargeting (control) siRNAs. Representative of 3 independent experiments.
(B) Dual-reporter cells stably expressing a DHFR-p21-mCherry fusion protein were differentiated in the presence of 10 μM TMP (to increase expression of p21) or DMSO (control). Representative of 2 independent experiments.
(C) Dual-reporter cells were transfected with cyclin D1 or nontargeting (control) siRNAs. Representative of 3 independent experiments.
(D) Dual-reporter cells were differentiated in the presence of a MEK inhibitor (PD0325091). Representative of 2 independent experiments.
(E) Dual-reporter cells were differentiated in reduced serum with and without EGF (bottom). Representative of 2 independent experiments.
(A-E) Histograms show the total time spent in G1 phase for each cell trace across all cell cycles for the respective experimental condition. Cells were induced to differentiate with the standard DMI protocol. Differentiation and cell cycle progression were assessed in the same manner as in Figure 3A.

Figure 7. Different optimal ranges of combined mitogenic and differentiation stimuli control the percent and total number of terminally differentiated cells
(A) Schematic of how increased proliferation before the PPARG threshold could control the number of adipocytes.
(B) Schematic of how the percent versus total number of differentiated cells can differ.
(C) Percent of undifferentiated/quiescent, undifferentiated/proliferating, and differentiated/post-mitotic cells were generated in three independent DMI-induced differentiation experiments.
(D) The maximum number of differentiated cells occurs in a “Goldilocks” range of mitogenic and adipogenic stimuli. See also Figure S7.

SUPPLEMENTARY MATERIAL

- **Supplementary Video 1:** Dual-reporter OP9 cells induced to undergo adipogenesis by addition of the commonly-used DMI adipogenic stimulus. Daughter 1 (blue trace) and

daughter 2 (red trace) only represent the product of the second mitosis (~58 hr) in the time trace. The outline represents the outline of nuclear segmentation based on the H2B channel. Geminin images, geminin trace (gray) and H2B are shown only for daughter 1.

- **Supplementary Video 2:** Dual-reporter OP9 cells transfected also with a CDK2 live-cell sensor induced to undergo adipogenesis by addition of the commonly-used DMI adipogenic stimulus.

- **7 Supplementary Figures**

SUPPLEMENTARY FIGURE LEGENDS

Figure S1. Additional validation of citrine-PPARG as a marker of differentiation commitment.

(A)The PPARG derivative and integral values are poorer predictors of differentiation, Traces from Figure 1B were smoothed using a Butterworth filter and a five-point stencil was applied to the smoothed traces to estimate the PPARG derivative at each timepoint. The PPARG derivative traces were then analyzed in a similar manner as in Figure 1E. The bins range from -300 to 300 in intervals of 50.

(B) The PPARG integral at each time point was estimated using the trapz() function in MATLAB (MathWorks). The integral values were then analyzed in a similar manner as described in Figure 1E. The bins range from 0 to 5x105 in intervals of 104. Note that both the derivative and integral are poor predictors for the final differentiated state. In the case of the derivative, the range between the lowest predicted probability and the highest predicted probability is smaller than found in Figure 1E. The integral values, although a good predictor for a single time point, suffers from the lack of consistency across timepoints, and a single integral value cannot be used to separate undifferentiated and differentiated cells for all timepoints.

(C) The analysis in Figure 1E was done for more time points that span the duration of the experiments and presented as a heatmap where rows represent a timepoint and the columns represents the PPARG bins as described in Figure 1E. The dotted line represents the estimated PPARG threshold for the experiment. The expanded analysis shows that the PPARG threshold remains stable throughout the experiment.

(D) The switch from PPARG low to PPARG high occurs over a relatively short time window. Blue traces represent unaligned population medians of the PPARG abundance (top) and PPARG derivative (bottom). The red trace represents the PPARG abundance (top) and PPARG derivative (bottom) after computationally aligning all traces by the time when the PPARG threshold is crossed and is represented by the zero timepoint. The dashed lines highlight the time window around the peak in the PPARG derivative of the aligned traces and suggests that the switch between PPARG low and PPARG high states occurs over a short window of about 4 hours. All shaded regions represent the interquartile range (25th-75th percentiles).

(E) Unaligned correlations of endpoint markers of adipogenesis to PPARG over a typical 4-day DMI differentiation experiment. PPARG timecourses from the cells that differentiated after 96 hours in Figure 1D were averaged. At each time point, the Pearson correlation coefficient between the unaligned PPARG values, and the endpoint immunofluorescence values for adipocyte markers was calculated.

Figure S2. The Geminin-based sensor behaves similarly to the Crl4-Cdt2-based sensor in marking the start of S-phase in OP9 cells.

(A) Dual reporter cells infected with a Crl4-Cdt2 sensor tagged with iRFP670. Cells were stimulated to differentiate using the DMI cocktalk, and timecourses from individual cells are plotted to compare the dynamics of the geminin sensor and Crl4-Cdt2 sensor.

(B) Comparison of median levels of the geminin and Crl4-Cdt2 sensors with t=0 marking the onset of S phase. Shaded regions represent the interquartile range (25th to 75th percentiles).

(C) Comparison of the median levels of geminin and Crl4-Cdt2 sensors at the onset of S-phases across multiple days of imaging. Shaded regions represent the interquartile range.

Figure S3. Additional results supporting Figure 2.

(A) Sub confluent plating conditions increase cell division events during adipogenesis. A comparison of the differentiation between dual reporter cells plated at two different cell densities. Dual reporter cells were differentiated using the standard DMI cocktail. Left, The plot represents the fraction of cells that are considered past the PPARG threshold at each time point for both cell density conditions. Right, A comparison of the fraction of dual reporter cells in S/G2/M phases of the cell cycle, as assessed by the geminin degron sensor, for both plating conditions.

(B) The number of mitotic events for both plating conditions are reported in the histogram as the fraction of cells observed with a given number of mitosis events. The 15,000 cells per well plating condition represents a standard differentiation protocol and yields high rates of differentiation and relatively low cell cycle activity. However, plating cells at a density of 5000 cells per well leads to a lower degree of differentiation and a higher degree of cell cycle activity. The live cell experiments in this manuscript are plated at a density of 5000 cells per well.

(C) Dilution through cell division does not significantly affect PPARG dynamics in differentiated cells. PPARG dynamics in differentiated cells were compared between cells that divided two (blue) or three (red) times in the span of the experiment, as indicated by the geminin degron sensor (right). Additionally, the selected cells all completed the last mitosis at similar times. PPARG (left) and geminin degron (right) traces were computationally aligned to the last mitosis time. Bold traces represent median values and the shaded region represents the 95th confidence interval of the median.

(D) The trade-off between continued proliferation and differentiation exists even in cells that have been selected for undergoing exactly two divisions during the timespan of a 96-hour live-cell experiment.

(E) A CDK2 sensor (orange trace) was added to the PPARG/geminin-degron dual reporter cells to create triple reporter cells. Triple reporter cells were differentiated using the standard DMI protocol, and a representative trace is shown. The yellow dot represents the time when the cell reached the PPARG threshold and irreversibly committed to the differentiated state. Representative of 2 independent experiments.

(F) Scatter plot showing the CDK2 activity versus PPARG level in each single cell at every time point. The red dashed line represents the PPARG threshold.

Figure S4. Experiments showing influence of cell cycle phase, number of previous cell cycles, and refreshing the stimulus/serum on differentiation.

Figure S5. Validation of the siRNA knockdown efficiency when cells were transfected at 48 hours after induction of adipogenesis.

(A) Cells were transfected with siRNA 48 hours after addition of the adipogenic DMI stimulus and knockdown efficiency was assessed 48 hours later (at the end of the 96-hour long time-lapse experiment). To validate the siRNA knockdown efficiency of p21 and CEBPA, cells were fixed with paraformaldehyde and immunostained for p21 or CEBPA levels.

(B) PPARG knockdown was assessed using the live cell citrine-PPARG signal.

Figure S6. Adipogenic stimuli initiate a competition between proliferation and differentiation during a gradually extending G1 phase.

(A) Analysis of timecourses in Figure 2B showing duration of G1 versus S/G2/M for differentiated and undifferentiated cells.

Representative of 3 independent experiments.
(B) Histogram of the difference between $G1_1$ and $G1_2$ for each cell from Figure 5B.
(C) Plot of G1 duration versus how long a cell had been exposed to the adipogenic (DMI) stimulus at the start of G1 for each cell from (A). Red line marks average G1 duration of all cells.

Figure S7. Titration of DMI versus FBS going up to higher maximal concentrations.

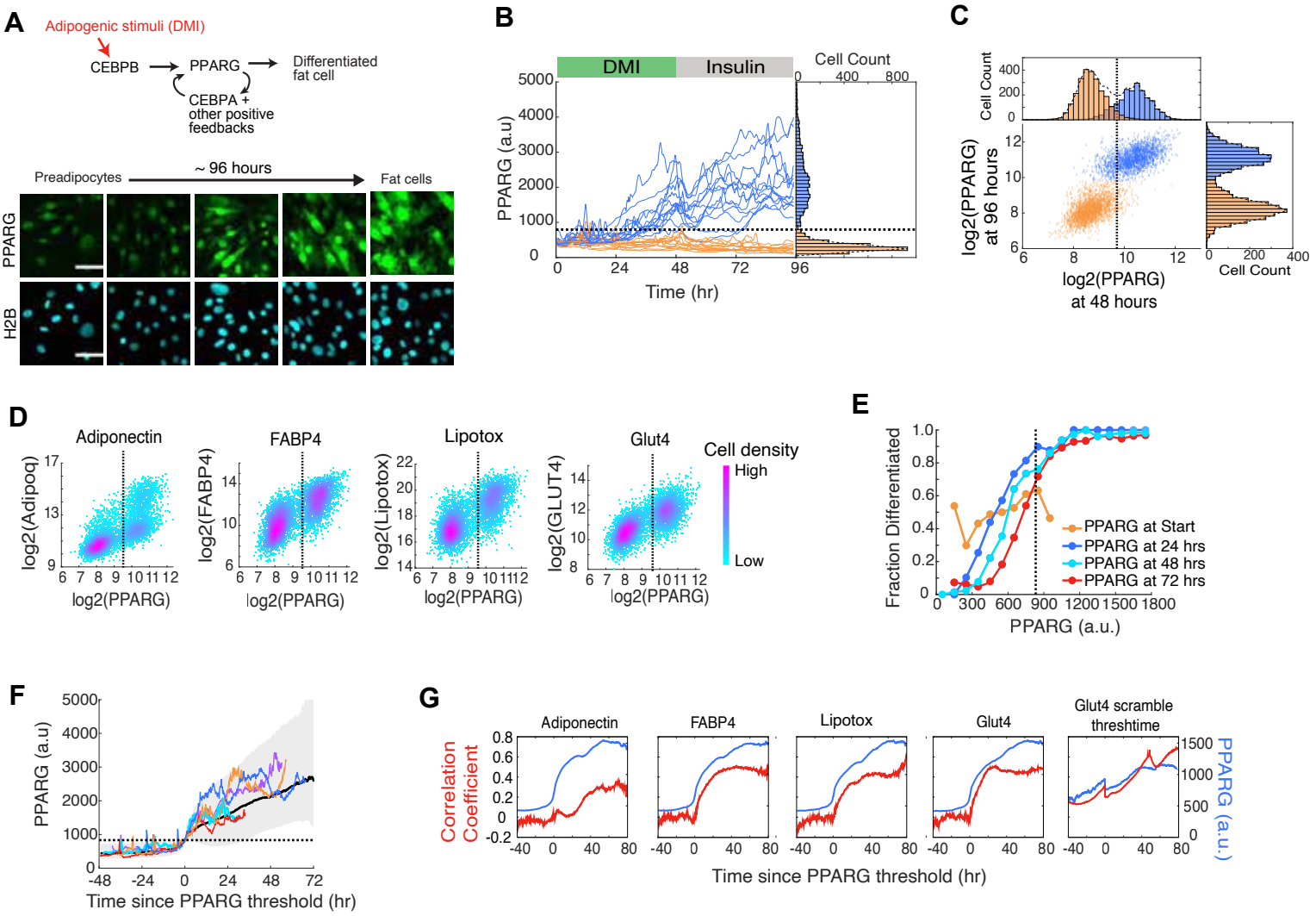

Figure 1. Measurement of the precise time when cells irreversibly commit to differentiate based on live single-cell analysis of endogenous expression levels of PPARG.

(A) Images of cells expressing endogenous citrine-PPARG that were differentiated using the standard 96-hour DMI protocol. Scale bar, 50 μm.

(B) Results of a typical experiment in which thousands of single cells were stimulated to differentiate. Thirty single-cell traces are shown as examples. Representative of 4 independent experiments.

(C) Scatter plot using data from (b) showing PPARG levels for each cell at 48 hours, just before the DMI stimulus was removed, and at 96 hours. Dashed black line represents the PPARG threshold (see Methods). Cells were defined as differentiated (blue) or undifferentiated (orange) by whether their PPARG levels were in the high or low intensity distributions, respectively.

(D) Citrine-PPARG cells were differentiated using the DMI protocol, and immunocytochemistry was performed at 96 hours for adipocyte markers (for each scatter plot: n > 4000 cells, representative of 2 independent experiments).

(E) The timecourses from (B) were split into equal-width bins by their PPARG values at 0, 24, 48, and 72 hours. The fraction of differentiated cells represents the number cells that crossed the PPARG threshold at the end of the experiment divided by the number of cells in the bin.

(F) Differentiating cells from (B) were computationally aligned so that the zero timepoint represents the time when the cell crossed the PPARG threshold. We plotted 5 representative single cell traces, the median (solid black line), and the 5th-95th percentile (shaded region).

(G) PPARG timecourses from the cells that differentiated after 96 hours in (D) were computationally aligned as in (F) and plotted (blue curves). At each aligned time point, the Pearson correlation coefficient between the aligned PPARG values and the endpoint immunofluorescence values for adipocyte markers was calculated (red curves). As a comparison, PPARG values for the Glut4 panel were aligned to a randomized PPARG threshold crossing point. The randomized crossing point was generated by scrambling the vector of measured threshold points for each cell so that each threshold point is matched with different cell.

(B-F) The dotted black line represents the calculated PPARG threshold for that experiment.

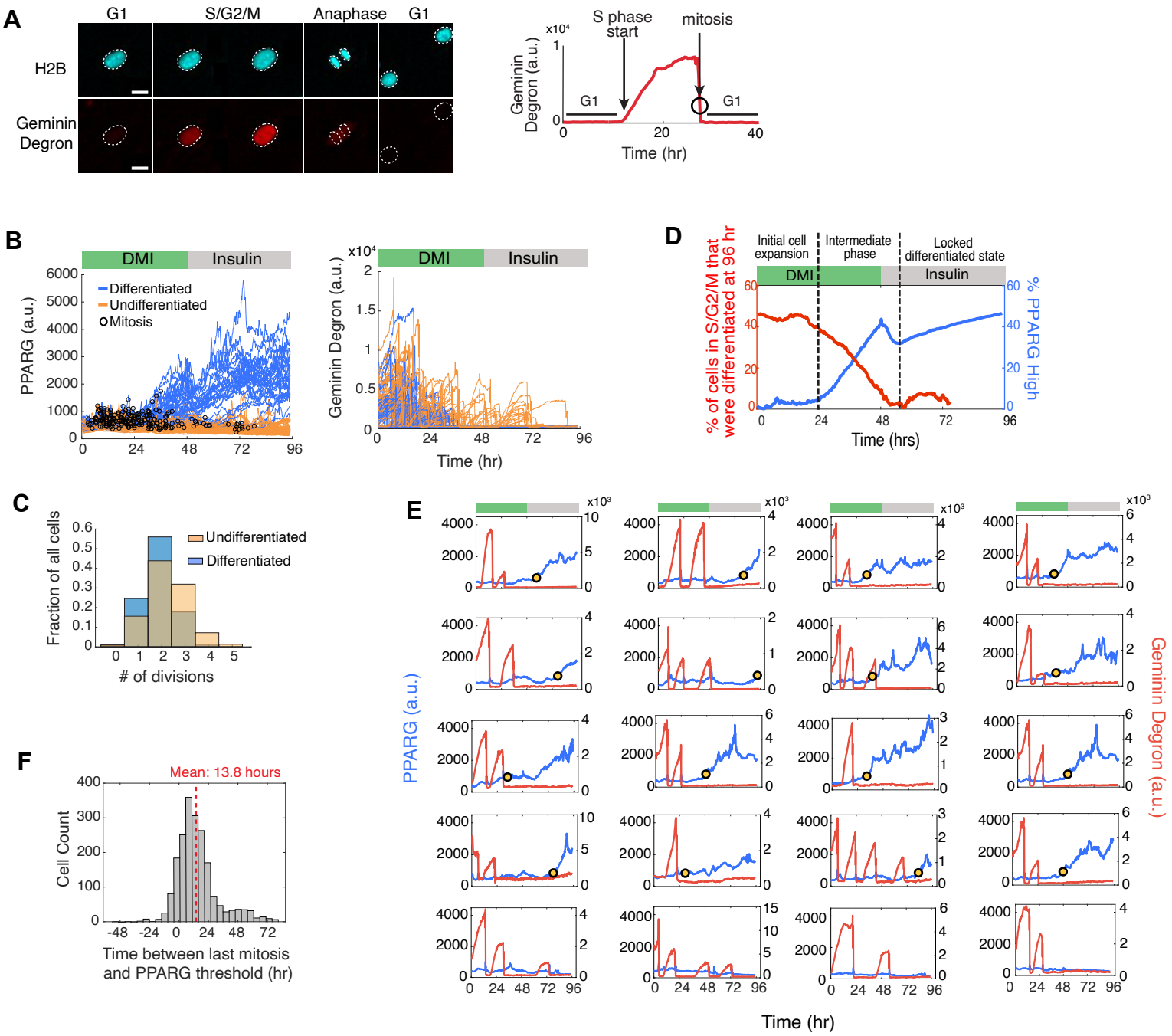

Figure 2. Development of a system to measure timecourses of cell cycle phases and terminal cell differentiation dynamics simultaneously in thousands of individual cells.

(A) Dual reporter cells were made by stably expressing H2B-mTurquoise(CFP) and geminin-degron-mCherry(RFP). Data from a representative single cell entering the cell cycle is shown. Anaphase is shown both by a split in the H2B-mTurquoise signal (top images) and by a sharp drop in geminin signal (bottom timecourse). Scale bar, 20 μm. White outlines mark the position of nuclei in cells after anaphase. To validate that the geminin degron sensor is suitable to monitor G1 length in the OP9 preadipocyte cell system, we compared its dynamics to that of a reporter of CRL4-Cdt2-mediated degradation that provides a more precise measure of the G1/S transition (Grant et al., 2018; Sakaue-Sawano et al., 2017) and confirmed that the dynamics of the two reporters are closely correlated (Figure S2).

(B) The dual reporter cells allow simultaneous measurement in thousands of single cells of differentiation state using PPARG levels (left) and cell cycle state using the geminin-degron sensor (right). The timepoints at which mitosis occurred were determined by using the split in H2B signal (black open circles). Representative of 4 independent experiments.

(C) Comparison of the number of observed mitotic events that occurred in cells that were differentiated versus cells that remained undifferentiate at the end of the 96-hour experiment shown in (B).

(D) Plot showing how the fraction of cells in S/G2/M (red) or with PPARG levels higher than the threshold (blue) varies during a 96-hour differentiation timecourse induced by DMI.

(E) Examples of PPARG (blue) and geminin-degron (red) timecourses obtained in the same single cell. Cells were stimulated to differentiate with DMI using the standard adipogenic protocol. The yellow dot in each plot marks the time at which that cell reached the PPARG threshold and irreversibly committed to the differentiated state.

(F) Histogram of the difference between the time when the PPARG threshold is crossed and when mitosis last occurred for each cell in the experiment shown in (B). Median value = 11 hours. The PPARG threshold is reached on average ~14 hours after the last mitosis is completed. Negative values indicate cells that reached the PPARG threshold before the last mitosis was completed.

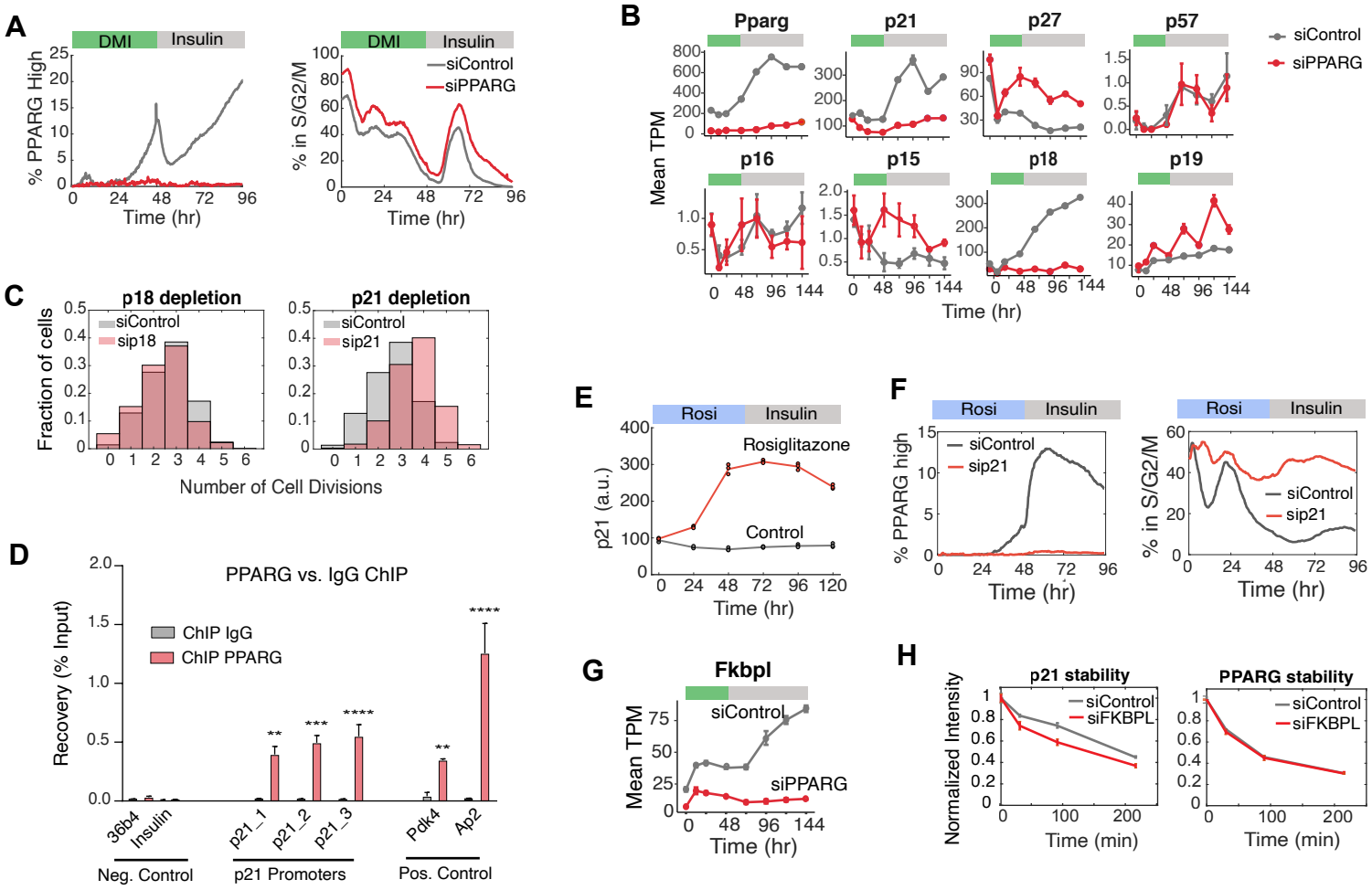

Figure 3. PPARG controls cell cycle activity in part by upregulating p21 expression.

(A-D) Application of the standard DMI cocktail for 48 hours was used to induce differentiation.

(A) Dual-reporter cells were transfected with PPARG or control siRNA and then stimulated to differentiate. The percent of cells in S/G2/M phases at each time point is calculated by counting the cells that expressed the geminin reporter during the 96-hour differentiation period divided by the total number of cells. The percent of PPARG high cells was assessed by counting the cells with PPARG levels above the threshold divided by the total number of cells at the respective timepoint. Cells were induced to differentiate with the standard DMI protocol. Approximately 5000 cells were analyzed per experiment. Representative of 3 independent experiments.

(B) Wildtype OP9 cells were transfected with PPARG or nontargeting siRNA and then stimulated to differentiate. RNA samples were collected every 24 hours for 144 hours. Data is plotted as transcripts per million (TPM), and mean ± 1 SD is shown for three replicates.

(C) Dual-reporter cells were transfected with p21, p18, or nontargeting siRNAs and stimulated to differentiate. The number of cell divisions per cell is reported in the normalized histograms. Representative of 2 independent experiments.

(D) Wildtype OP9 cells were stimulated with rosiglitazone for 48 hours. Chromatin immunoprecipitation (ChIP) of PPARG was performed followed by qPCR. Three sites on the p21 promoter are shown. The promoters of insulin and Arbp/36b4 served as negative controls, and known PPARG target genes Fabp4/aP2 and Pdk4 (pyruvate dehydrogenase kinase, isoenzyme 4) were used as positive controls. Data are normalized to a nontarget genomic site and IgG enrichment. Two biological experiments were used. Two-way ANOVA with Bonferroni's multiple comparisons test was applied for statistical analysis. Values represent means ± SEM. $p<0.05$, ** $p<0.01$, ***$p<0.001$, ****$p<0.0001$.

(E) Wildtype OP9 cells were stimulated to differentiate by addition of 1 μM rosiglitazone. p21 levels were measured by fixing and staining cells at subsequent times. Approximately 5000 cells were analyzed per experiment. Data is plotted as mean (line) along with the values for each of the three experiments (points).

(F) Wildtype OP9 cells were transfected with p21 or Control siRNA and stimulated to differentiate by addition of 1 μM rosiglitazone. Differentiation and cell cycle progression were assessed in the same manner as in Figure 3A.

(G) FKBPL expression under nontargeting vs PPARG knockdown were obtained from the RNA-seq data in (B). Data reported as TPM, mean ± 1 SD.

(H) Wildtype OP9 cells were transfected with FKBPL or nontargeting siRNAs, and DMI was added to initiate differentiation. Stability of p21 and PPARG were assessed by adding 30 μM cycloheximide to the media 24 hours after DMI addition and then fixing and staining for protein levels at different subsequent times. Approximately 5000 cells were analyzed per experiment. Data is plotted as mean ± 1 SD of three replicates.

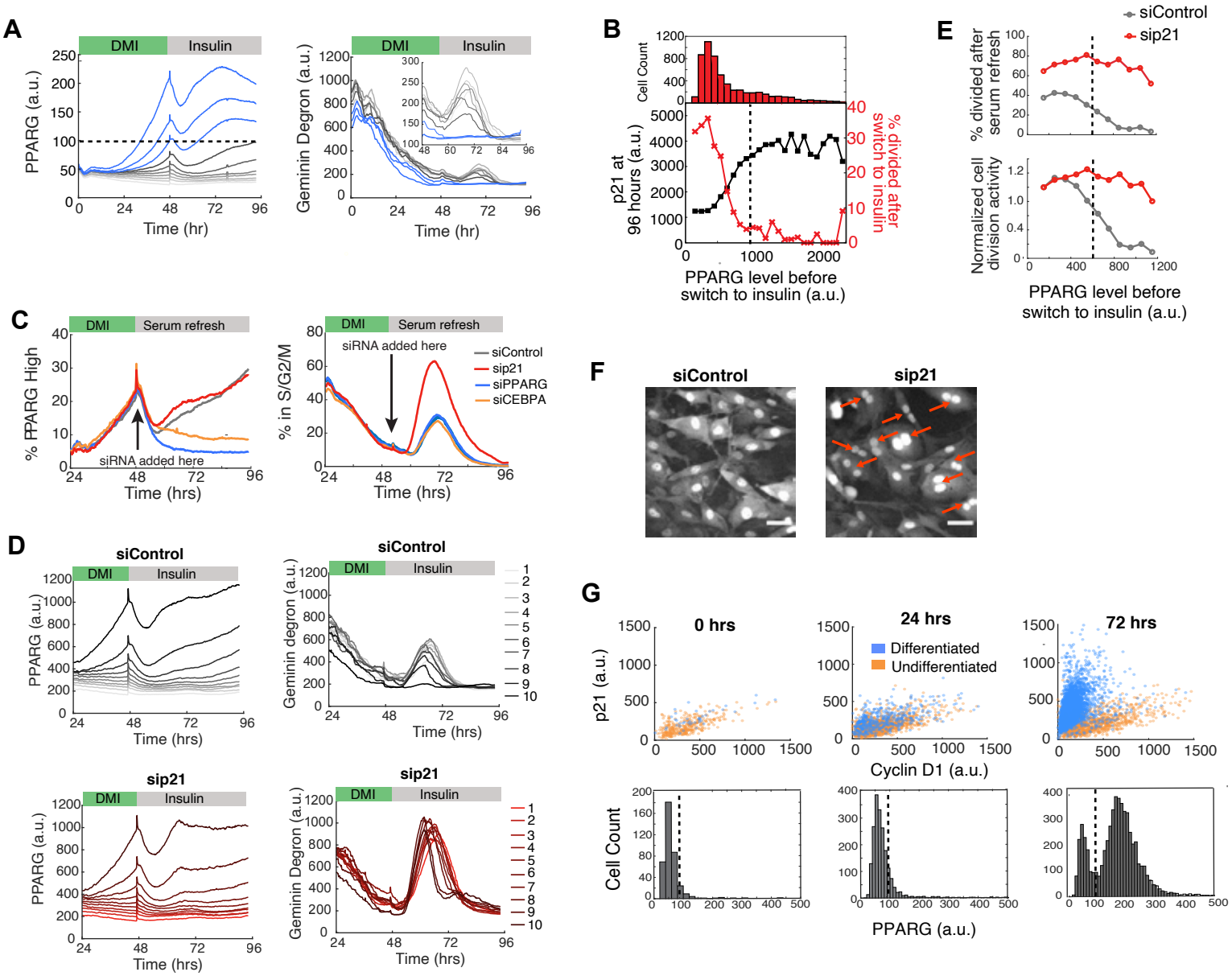

Figure 4. Cells crossing the PPARG threshold for differentiation become unresponsive to mitogenic stimulation and are locked into a post-mitotic state by p21.

(A)Citrine-PPARG and geminin levels were measured in dual-reporter cells in response to media replacement at 48 hours. Cells were separated into ten bins based on their PPARG levels at 48 hours. Plotted lines show mean values for each bin. Inset shows the geminin-degron signal between 48-96 hours. Representative of 2 independent experiments.

(B) PPARG values before serum refresh were binned from 100 to 2500 a.u. in 100 a.u. increments. The plot shows for each bin the fraction of cells with a minimum of one division (measured by a split in nuclear H2B signal, red) and the final p21 level (black) and in response to serum refresh. The histogram shows the number of cells in each bin. The dotted black line shows the PPARG threshold for this experiment. Data from experiment in (A).

(C) PPARG, CEBPA, p21, and nontargeting siRNA were transfected into the dual-reporter cells at 48 hours after DMI addition. siRNA knockdown efficiency is shown in Figure S6. Representative of 3 independent experiments.

(D) A similar analysis as described in (A) was performed on the nontargeting and p21 knockdown conditions from (C).

(E) Left, A similar analysis as in (B) was performed on the nontargeting and p21 knockout conditions from (D). Right, the same data normalized to the first PPARG bin.

(F) Images of control and p21-knockdown cells from (C) obtained 48 hours after siRNA transfection (at 96 hours). Red arrows indicate representative multi-nucleated cells. Scale bar, 50 μm.

(G) OP9 cells were induced to differentiate with rosiglitazone. Cyclin D1, p21 and PPARG levels were assessed by immunocytochemistry. The PPARG threshold for the whole experiment (dotted black line) was calculated at the end of the 96-hour differentiation protocol. Representative of 2 independent experiments.

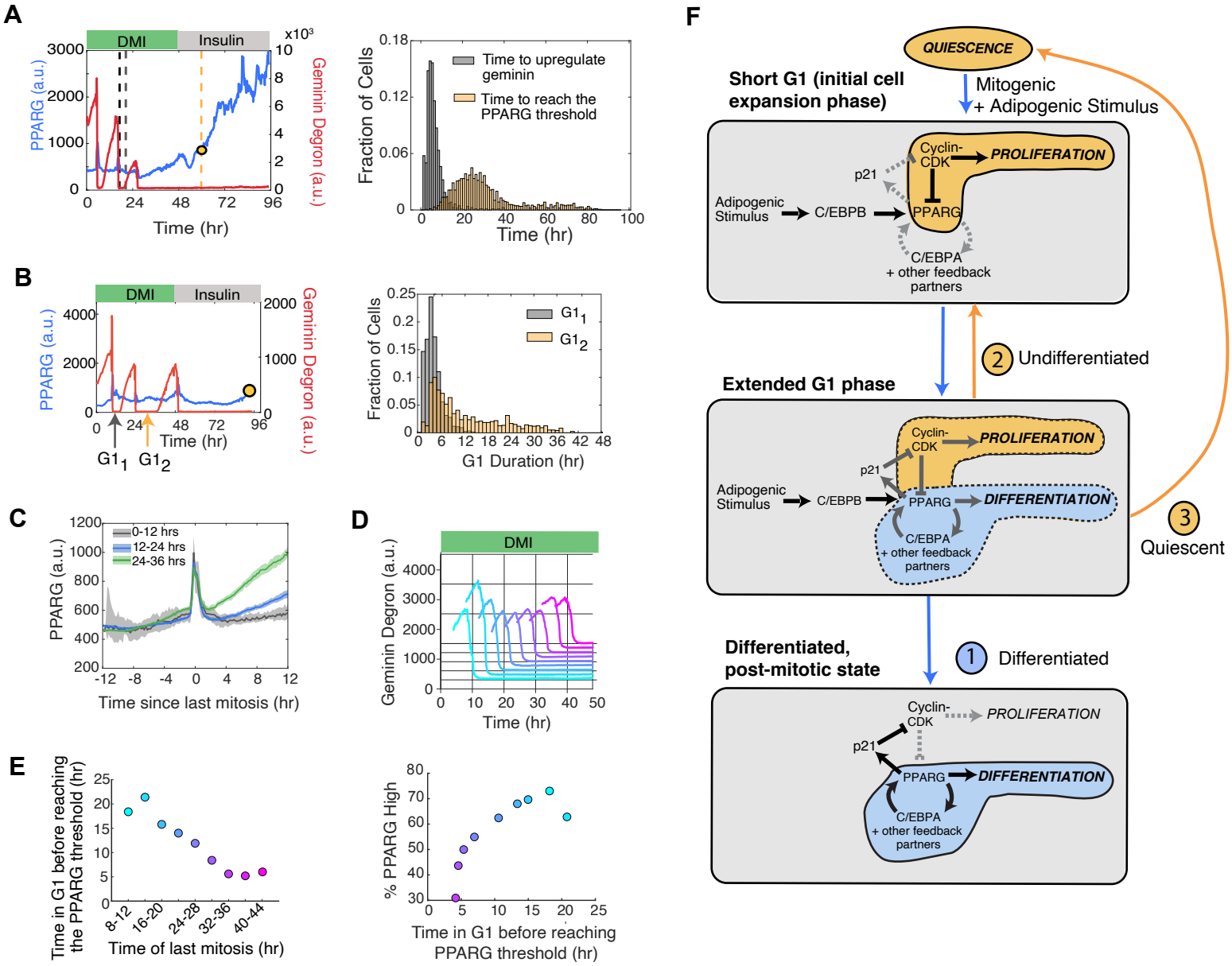

Figure 5. Adipogenic stimuli initiate a competition between proliferation and differentiation during a gradually extending G1 phase.
(A) Comparison of the time to commit to the next cell cycle (marked by upregulation of geminin) versus time to commit to differentiation in cells that underwent 2-3 mitoses before differentiating. *Right,* Schematic showing that the end of the second-to-last mitosis is used as the starting reference time for each cell. *Left,* histograms comparing the two times measured in the same cell (data from Figure 2B, n > 4000 cells, representative of 4 replicates).
(B) *Left,* Schematic showing which G1-periods were compared. *Right,* Histograms of the durations of the 1st and 2nd G1-periods in cells from (A) that have undergone at least 3 divisions.See also Figure S6.
(C) Differentiated cells from (A) were separated into three groups based on when they last exited mitosis. The traces were aligned by the last mitosis frame. The median PPARG levels were plotted for each group (dark line). Shaded region represents the 95th confidence interval.
(D) Timecourses from (A) were categorized into 9 bins based on time of last mitosis. The geminin peak for each bin is plotted to illustrate when the last mitosis occurred relative to addition of the adipogenic (DMI) stimulus.
(E) *Left,* Plot showing the average time of the last mitosis versus the average time it took for cells in that bin to increase PPARG levels to the differentiation commitment point. *Right,* Plot of binned cells from (E) showing the average time spent in G1 versus the percent of cells in that bin that were PPARG high.
(F) Schematic of the three stages of G1-extension, in response to an adipogenic (DMI) stimulus. During the intermediate phase of G1-extension, stochastic competition between proliferation and differentiation causes cells to probabilistically exit into a differentiated or proliferating state. This phase defines how many differentiated cells are generated on average from a precursor cell.

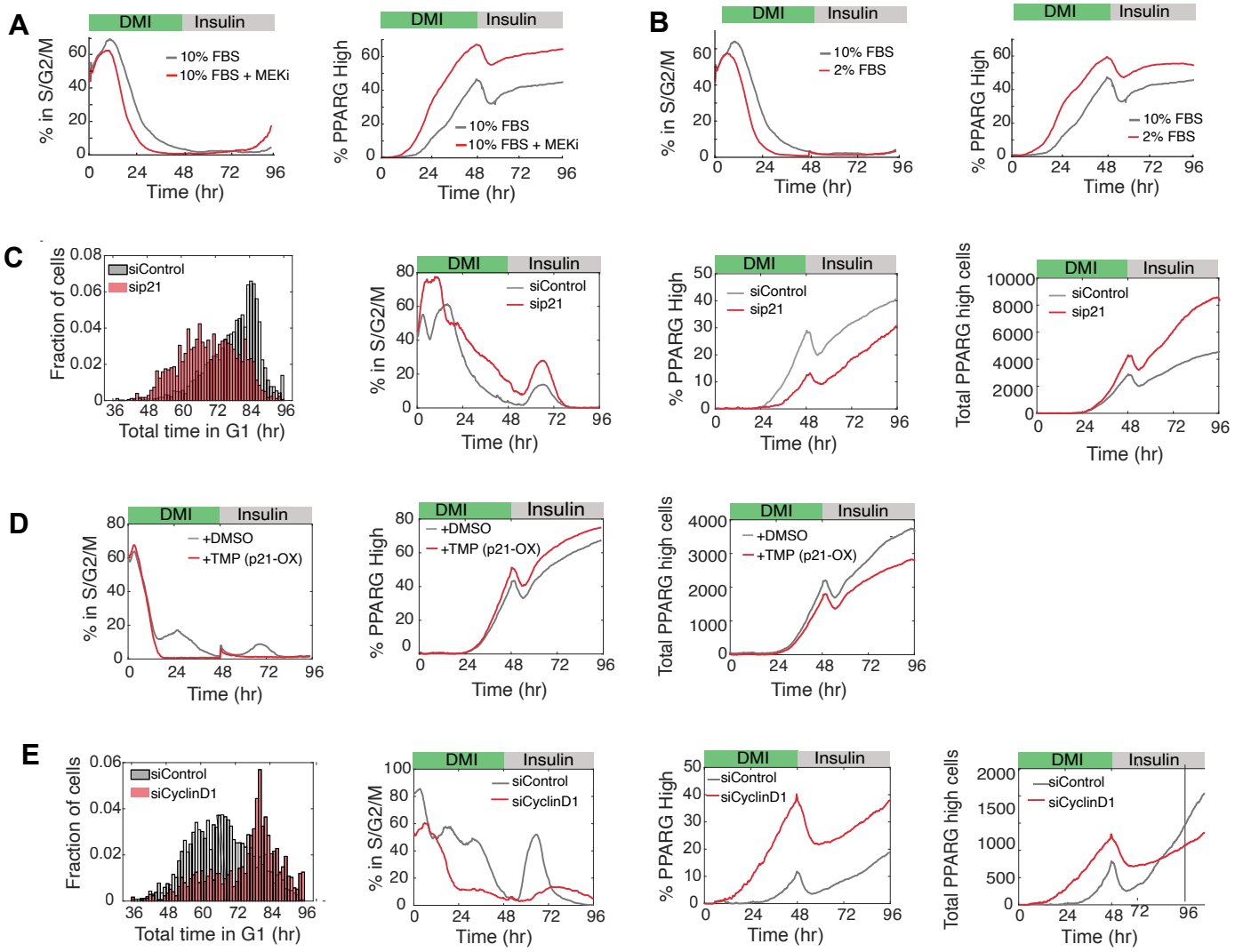

Figure 6. Regulation of G1 duration oppositely controls the percent versus the total number of terminally differentiated cells.
(A) Dual-reporter cells were transfected with p21 or nontargeting (control) siRNAs. Representative of 3 independent experiments.
(B) Dual-reporter cells stably expressing a DHFR-p21-mCherry fusion protein were differentiated in the presence of 10 μM TMP (to increase expression of p21) or DMSO (control). Representative of 2 independent experiments.
(C) Dual-reporter cells were transfected with cyclin D1 or nontargeting (control) siRNAs. Representative of 3 independent experiments.
(D) Dual-reporter cells were differentiated in the presence of a MEK inhibitor (PD0325091). Representative of 2 independent experiments.
(E) Dual-reporter cells were differentiated in reduced serum with and without EGF (bottom). Representative of 2 independent experiments.
(A-E) Histograms show the total time spent in G1 phase for each cell trace across all cell cycles for the respective experimental condition. Cells were induced to differentiate with the standard DMI protocol. Differentiation and cell cycle progression were assessed in the same manner as in Figure 3A.

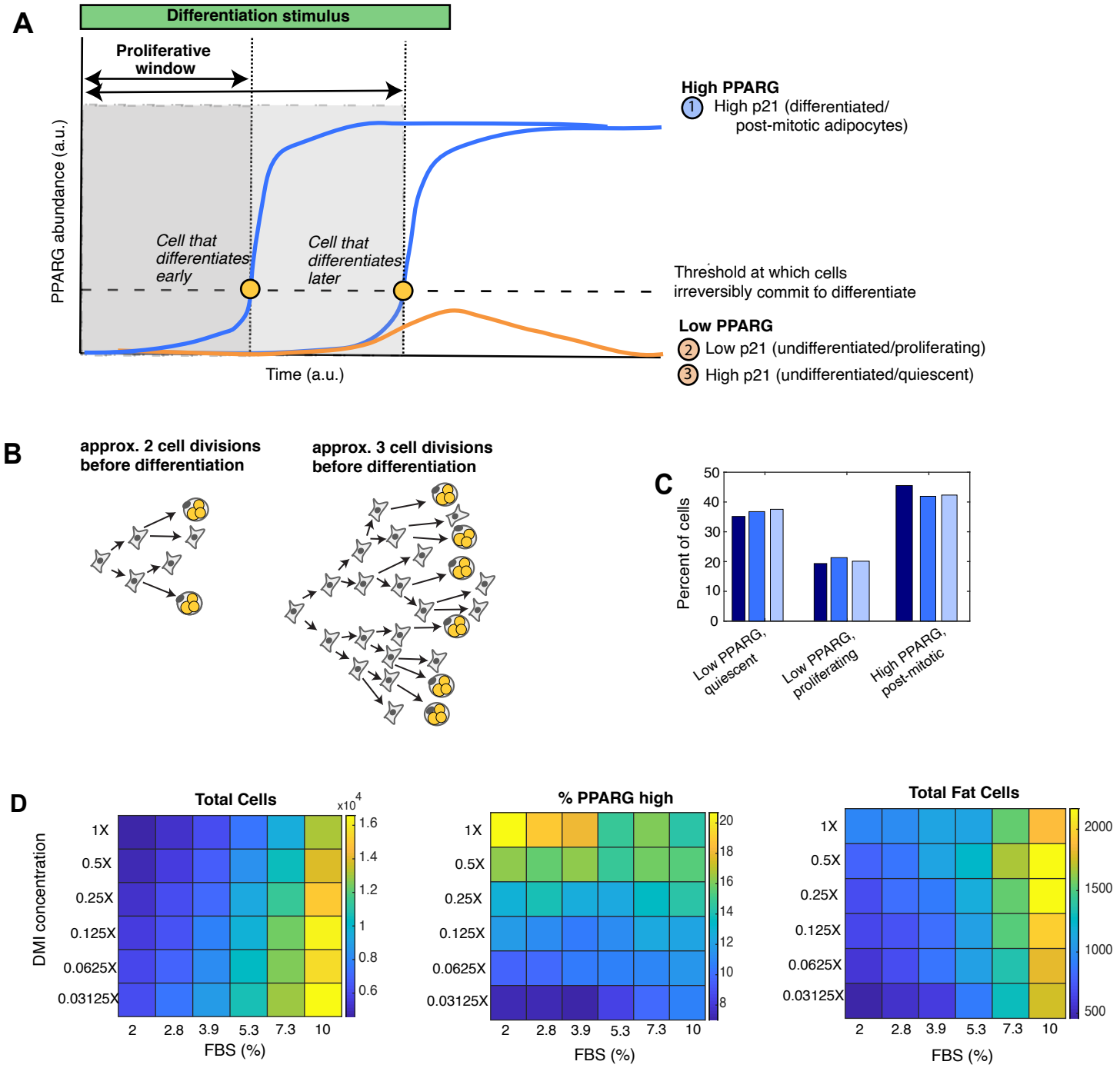

Figure 7. Different optimal ranges of combined mitogenic and differentiation stimuli control the percent and total number of terminally differentiated cells

(A) Schematic of how increased proliferation before the PPARG threshold could control the number of adipocytes.

(B) Schematic of how the percent versus total number of differentiated cells can differ.

(C) Percent of undifferentiated/quiescent, undifferentiated/proliferating, and differentiated/post-mitotic cells were generated in three independent DMI-induced differentiation experiments.

(D) The maximum number of differentiated cells occurs in a “Goldilocks” range of mitogenic and adipogenic stimuli. See also Figure S7.